Distributed deformation along the subduction plate interface: The role of tectonic mélanges

Hugues Raimbourg, Vincent Famin, Giulia Palazzin, Asuka Yamaguchi, Romain Augier, Yujin Kitamura, Arito Sakaguchi

Distributed deformation along the subduction plate interface: the role of tectonic mélanges

Hugues Raimbourg[a,b,c], Vincent Famin[d], Giulia Palazzin, Asuka Yamaguchi[e], Romain Augier[a,b,c], Yujin Kitamura[f], Arito Sakaguchi[g]

(a) Université d'Orléans, ISTO, UMR 7327, 45071 Orléans, France

(b) CNRS, ISTO, UMR 7327, 45071 Orléans, France

(c) BRGM, ISTO, UMR 7327, BP 36009, 45060 Orléans, France

(d) Laboratoire Géosciences Réunion, Université de La Réunion, IPGP, Sorbonne Paris Cité, UMR 7154 CNRS, Saint-Denis, La Réunion, France

(e) Department of Ocean Floor Geoscience, Atmosphere and Ocean Research Institute, University of Tokyo 5-1-5 Kashiwanoha, Kashiwa, Chiba 277-8564, Japan

(f) Graduate School of Science and Engineering, University of Kagoshima, 1-21-40 Korimoto Kagoshima-city Kagoshima 890-0065, Japan

(g) Graduate School of Sciences and Technology for Innovation, Faculty of Science, University of Yamaguchi, 1677-1 Yoshida, Yamaguchi-shi, Yamaguchi 753-8511, Japan

Corresponding author: Hugues Raimbourg (hugues.raimbourg@univ-orleans.fr)

1-Abstract

Recent geophysical monitoring of subduction zones has unraveled a complete spectrum of plate coupling behaviors, from coupled portions rupturing during earthquakes to decoupled portions slipping aseismically. However, the deformation mechanisms and the exhumed rock corresponding to these contrasted behaviors are not yet identified. Tectonic mélange zones are thought to play a major role in the deformation of the plate interface as they represent remnants of the subducted plate scraped off by the overriding plate. In this work we examine several tectonic mélange zones (Hyuga, Okitsu, Mugi) from the Shimanto Belt, an accretionary prism in southwest Japan connecting to the active Nankai subduction zone. These tectonic mélange zones have a block-in-matrix structure, with lenses of sandstones and basalts within a metapelitic matrix, and their deformation is distributed over zones of hundreds of meters in thickness. In addition, the examples of mélange considered here are bounded by sharp faults, some of them bearing pseudotachylyte layers, so that distributed deformation within the mélange and localized deformation on its boundary are juxtaposed. Distributed deformation involves the development of a foliation, as well as of a pervasive network of macroscopic and microscopic shear zones. Along with slip on this network, strain proceeds by fracturing and precipitation of quartz, in long veins parallel to the foliation or in smaller cracks perpendicular to stretching and forming in the neck of competent lenses of sandstones or former quartz veins. The analysis of shear band kinematics shows in all three examples a dominant, top-to-the-trench sense of shear, consistent with deformation along the plate boundary during subduction. Moreover, most shear zones, when foliation is restored back to syn-subduction position, are extensional structures. Finally, the geometry and kinematics of the mélange-bounding faults, as well as radiometric constraints, show that in most cases the faults (=localized structures) were formed during a later stage than mélange internal deformation. These findings bear several consequences on the structure and dynamics of the subduction plate boundary at seismogenic depths. First, there is no support for a model of plate boundary fault zone composed simultaneously

of localized slip zones and domains of more distributed deformation. Second, rather than proposed models of underplating, where all deformation is localized into the thrusts bounding the tectonic sheets, we suggest that underplating was to a large extent accommodated by distributed deformation within the mélange sheets. This underplating model accounts for (i) the large amount of strain within the mélange, (ii) the absence of contractional structures during underplating, (iii) thinning of the mélange required by the network of extensional shear bands and stretched boudins. Third, mélanges appear as likely candidates for portions of the plate interface deforming by aseismic slip. The seismic vs. aseismic character of the plate interface might depend on the ability of sediments on top of the subducting plate to undergo distributed strain, which in turn depends on the efficiency of pressure solution to operate.

Highlights

1) Tectonic mélanges in fossil subduction zones reveal deep deformation processes

2) Distributed strain combines pressure-solution in quartz and slip on phyllosilicates

3) Underthrusting along subduction interface results from distributed strain

4) A network of extensional shear zones formed during mélange underplating

5) Fault zones, including pseudotachylytes, formed after underplating

Keywords

Subduction zones; deformation; rheology; pressure solution; underplating

2-Introduction

The use of rate-and-state friction laws (Dieterich, 1994; Ruina, 1983) has proved to be a very powerful theoretical tool to reproduce the seismic behavior that occurs along plate boundaries. Earthquake cycles on strike-slip (Lapusta and Rice, 2003; Tse and Rice, 1986) or subduction faults (Kato and Hirasawa, 1997; Stuart, 1988) have been successfully modelled using imposed depth variations of friction parameters (a-b). Similarly to these models, slow-slip events (SSE), which occur towards the shallow or deep domain of the seismogenic zone (Bilek and Lay, 2018; Dragert et al., 2001; Obara et al., 2004; Obara and Kato, 2016; Ozawa et al., 2007; Peng and Gomberg, 2010; Saffer and Wallace, 2015; Schwartz and Rokosky, 2007), are commonly envisioned in the mechanical framework of friction. For example, assuming a transition from a velocity-weakening to a velocity-strengthening behavior towards the downdip limit of the seismogenic zone results in the spontaneous generation of SSE in this transition zone (Liu and Rice, 2005, 2007). From mega-earthquakes to SSE, the plate interface is therefore usually modelled as a frictional interface down to temperatures of 350-450°C where viscous processes are thermally activated (Hyndman et al., 1997; Oleskevich et al., 1999).

Considering the plate interface as a frictional surface, the corresponding natural structures are faults, which have been thoroughly studied and described in transcurrent settings (Chester and Logan, 1986; Faulkner et al., 2010; Faulkner et al., 2003; Sibson, 2003; Wibberley and Shimamoto, 2003). Common models of faults revolve around a single or a small number of high-strain fault cores or fault gouge bands (=principal slip zones), surrounded by a damage zone. The thickness of the principal slip zones which accommodate most of the strain, although depending on the nature of the wall rock (Faulkner et al., 2010; Faulkner et al., 2003), is always thinner than a few meters and often restricted to a dm- to cm-thick layer of gouge or ultracataclasite (Sibson, 2003; Wibberley and Shimamoto, 2003).

In subduction zones, seismic discontinuities interpreted as plate boundary décollements have been drilled at relatively shallow depths (<1km below seafloor). The NE Japan margin (Chester et al., 2013),

the Nankai Trough (Shipboard Scientific Party, 1991, 2001) or the Barbados (Maltman et al., 1997) décollements consist of a 5-30m thick zone concentrating, with respect to surrounding rocks, abundant deformation structures such as breccia and faults (Nankai Trough), or clay scaly fabrics (Barbados and NE Japan). Observations at larger depths are beyond the reach of active margin drilling and rely on fossil structures (e.g. (Rowe et al., 2013; Vannucchi et al., 2012a)). In the Shimanto Belt, the Cretaceous to Mesozoic accretionary prism bordering SW Japan, the Nobeoka Tectonic Line (NTL) is a large-scale, out-of-sequence fault that accommodated tens of km of displacement (Raimbourg et al., 2014a). Even though a damage zone is observable in the footwall, all the displacement is localized on a few cm thick cataclastic fault core (Kondo et al., 2005; Mukoyoshi et al., 2009). A network of sharp faults, with principal slip zones thicknesses of less than 10mm and displacement larger than a few kilometers, has also been recognized in the same belt on Shikoku Island (Mukoyoshi et al., 2006). In the Kodiak accretionary prism in Alaska, near Pasagshak Point, very-fine grained, black fault-rocks form a dm-thick horizon traceable over kilometers that was interpreted as an ancient pseudotachylyte layer (Meneghini et al., 2010; Rowe et al., 2011; Rowe et al., 2005). In the Shimanto Belt, similar cm-thick pseudotachylytes have been described, either forming tectonic boundaries or crosscutting preexisting boundaries (Ikesawa et al., 2003; Mukoyoshi et al., 2006; Ujiie et al., 2007).

In contrast to these very narrow zones of deformation, tectonic units of disrupted metasedimentary sequences, called tectonic mélanges, coexist with the cataclastic zones described above in many acretionary prisms such as Kodiak, the Shimanto Belt, the Franciscan Complex, the Apennines or the Otago Schists (Connelly, 1978; Cowan, 1985; Fagereng and Sibson, 2010; Festa et al., 2012; Kimura and Mukai, 1991; Meneghini et al., 2009; Moore and Wheeler, 1978; Wakabayashi, 2011). Tectonic mélanges have a block-in-matrix structure resulting from pervasive deformation and contain various deformation structures, such as cataclastic bands and shear zones, pressure-solution foliations and mineralized veins (Fisher and Byrne, 1987, 1990; Kimura and Mukai, 1991; Kitamura and Kimura, 2012). Some examples show thicknesses as large as several hundreds of meters, as noted in Rowe et

al. (2013), e.g. in the Shimanto Belt (Ikesawa et al., 2005; Imai et al., 1975; Kitamura et al., 2005; Okumura et al., 2010; Saito et al., 1996; Sakaguchi et al., 2006) or the Apennines (Vannucchi et al., 2010), while other mélanges are thicker than 1km, e.g. in the Northern Alps (Bachmann et al., 2009) or in Alaska (Byrne and Fisher, 1990; Fisher and Byrne, 1987).

Tectonic mélanges appear therefore as thick deformation zones, where strain is distributed over hundreds of meters of thickness, contrasting with localized faults (Cowan, 1974). A major question concerns the relationship between these different deformation structures. One possible view is to interpret all deformation structures, tectonic mélanges (=damage zones) as well as fault zones and pseudotachylyte layers (=principal strain zones), as part of a single deformation zone (Rowe et al., 2013). Following this line of thought, Alaskan mélanges have been interpreted as shear beneath a master décollement (Byrne and Fisher, 1990; Fisher and Byrne, 1987, 1990), and the Hyuga Tectonic mélange on eastern Kyushu coast has been interpreted as the damage zone of the NTL, a sharp fault constituting its roof thrust (Kondo et al., 2005).

In this work we reexamine this interpretation of tectonic mélanges as low-strain zones within a plate boundary zone, using new structural and microstructural data acquired through several tectonic mélanges from the Shimanto Belt in Japan. Compiling these structural and microstructural data with other arguments such as radiometric constraints, we show that the deformation recorded within mélanges corresponds to a new mode of underplating. We then discuss the chronological relationship between localized and distributed deformation.

3 Geological setting

3.1 General architecture of the Shimanto Belt and studied areas

The Shimanto Belt is a partly exhumed accretionary prism forming the southern border of Japan and extending seaward into the active Nankai Trough margin (Kimura et al., 2016) (Figure 1). Biostratigraphic ages range from Cretaceaous to Miocene and show an overall younging trend from

north to south (Taira, 1981; Taira et al., 1988; Taira et al., 1980a; Taira et al., 1980b). The belt is schematically divided into a northern Cretaceous and a southern Cenozoic subbelts, separated by a large-scale fault known as the NTL, on Kyushu. The Shimanto Belt consists mainly of a sedimentary accretionary wedge, predominantly composed of sandstones and mudstones in variable proportions. Other deep seafloor typical lithologies, such as red shales, radiolarites or basalts are volumetrically much less abundant. Most of the sediments preserve their sedimentary bedding, defining "coherent" units, in contrast with less abundant units of broken formations or tectonic mélanges (Festa et al., 2012). The general architecture of the wedge is an imbrication of km-scale units, separated by sharp contacts most often not observable on the field with an overall bedding or foliation dip to the north or northwest. The dip is commonly around 30° or less on Kyushu (especially in the Northern Belt and in the Hyuga mélange) and much larger on Shikoku, where most units are close to the vertical (Raimbourg et al., 2017).

From west to east of the Simanto Belt, tectonic mélanges analyzed here are the Hyuga tectonic mélange on eastern Kyushu (Palazzin et al., 2016; Raimbourg et al., 2014a; Raimbourg et al., 2017) (Figure *2*), the Okitsu and Kure mélanges on western Shikoku (Ikesawa et al., 2003; Mukoyoshi et al., 2006; Sakaguchi, 1999a, 2003; Sakaguchi et al., 2006; Taira et al., 1988) and the Mugi mélange on eastern Shikoku (Ikesawa et al., 2005; Kitamura et al., 2005) (Figure *3*).

Biostratigraphic ages in the matrix are Late Eocene to Early Oligocene for the Hyuga mélange (Sakai et al., 1984), and Campanian to early Maastrichtian (for the youngest shales) for the Shikoku mélanges (Hara et al., 2017; Taira et al., 1988). U/Pb dating of zircon grains from intercalated tuff layers within the Mugi mélange yielded Late Cretaceous to Early Paleogene ages (Shibata et al., 2008).

All these mélanges present a highly disrupted fabric. In most of their volume, the mélanges are strictly made of sedimentary material, with blocks of sandstones ± tuff layers embedded in a pelitic matrix. Locally, pods of basalts are also present, along with lenses of deep seafloor sediments such as radiolarites or red shales (Figure 2), in a pelitic matrix. The blocks of sandstones have a variable size,

from mm- to m-scales. Basalts, which show a preserved pillow-lava structure in some instances such as Mugi, form larger m- to tens-of-meters sized lenses. In some mélanges, the recognition of complete or partial ocean-floor stratigraphy (i.e. the succession of pillowed basalts, radiolariarian cherts, red pelagic clays and varicolored hemipelagic shales (Taira et al., 1988)), and the occurrence of fault zones along the basal (i.e. southern) boundaries of basalt layers (e.g. (Kitamura et al., 2005)) led to the interpretation of mélange zones as a stack of several thrust sheets, each of them soled by a layer of basalts. For example, three thrust sheets are described in the Okitsu mélange (Sakaguchi, 2003), five thrust sheets in the Mugi mélange (Kitamura et al., 2005), while the internal subdivision of the Hyuga mélange is still unclear but several distinct lenses of basalts are present in the tectonic pile (Murata, 1994, 1997, 1999). In this respect, as the different blocks present in the mélange matrix originate from *in situ* tectonic dismembering of the stratigraphic succession on top of the oceanic plate, they are not strictly speaking “exotic” blocks and the mélange proper denomination should be “chaotic formation” (Festa et al., 2012). Nevertheless, for the sake of consistency with existing literature on Shimanto, we hereafter keep the term “tectonic mélange”.

3.2 P-T conditions of deformation

Metamorphic temperatures within the Hyuga mélange inferred from vitrinite reflectance, illite crystallinity and Raman spectra of carbonaceous matter (RSCM) geothermometers yielded similar values of ca. 240-270°C (Hara and Kimura, 2008; Kondo et al., 2005; Mukoyoshi et al., 2009; Raimbourg et al., 2017) (Table 1). On Shikoku, paleotemperatures in the Kure and Okitsu mélanges are of ~225°C (Mukoyoshi et al., 2006) and 230-265°C (this study, (Sakaguchi, 1999b), respectively. On the basis of paleotemperatures, the Mugi mélange is divided into a “hotter” upper unit at ~220°C and a “colder” lower unit at 165-185°C (Ikesawa et al., 2005). Despite small discrepancies among geothermometers, both vitrinite reflectance and RSCM analyses show that maximum temperatures are, in descending order, Hyuga, Okitsu/Kure/upper Mugi and lower Mugi.

Pressure estimates for the Huyga mélange, loosely constrained by the metamorphic assemblage prehnite–pumpellyite in greenstones, are of the order of 3-5kbar (Toriumi and Teruya, 1988). In Shikoku mélanges, some pressure estimates are primarily based on coexisting methane-rich and water-rich fluid inclusions, and by assuming equilibrium/coeval trapping (e.g. Matsumura et al. (2003)). This hypothesis was shown to be invalid in the Hyuga mélange (Raimbourg et al., 2014b) and in the Okitsu mélange (Sakaguchi, 1999a), so that such pressure estimates are not reliable. Other methods using only water-rich fluid inclusions trapped in syn-tectonic veins give an estimate of the minimum temperature and fluid pressure that accompanied deformation (Kondo et al., 2005; Matsumura et al., 2003; Raimbourg et al., 2015). The comparison of maximum temperature of deformation in the rock (from vitrinite reflectance, illite crystallinity or RSCM geothermometers) and minimum temperature in the fluid (homogenization temperature of water-rich fluid inclusions) are close in value. As a consequence, the pressure that can be deduced from the water-rich fluid inclusions is close to the liquid-vapor curve (where homogenization occurs) hence systematically very low (1-2kbar), which is interpreted as the result of either (i) cycles of fluid pressure and precipitation of the veins/fluid inclusion trapping at low points of the cycles or (ii) reequilibration of fluid inclusions during uplift (Raimbourg et al., 2018).

3.3 Geodynamical evolution and structural settings of deformation

The first-order architecture of the Shimanto Belt, with a younging trend in stratigraphic ages towards the south, is the main argument in favor of a model of progressive accretion and growth from Cretaceous to Miocene. Such a model was disputed by the recognition of a collision stage in Early Miocene, based on geological observations on-land Japan of a belt-wide unconformity (Charvet, 2013; Charvet and Fabbri, 1987; Sakai, 1988; Sakai, 1985; Sakamoto, 1977; Tanaka, 1977) and on paleogeographic reconstructions showing the collision of SW Japan with the Northern Philippines Sea Arc (Wu et al., 2016). The collision was responsible for the development of a vertical foliation, as a result of horizontal shortening, in the Cenozoic part of the belt on western Shikoku (Raimbourg et al.,

2017). Additionally, this work suggested that the collision stage also affected more internal domains of the belt, through for example the movement on the NTL on Kyushu or through large-scale tilting of the tectonic units on Shikoku.

Most studies focused on mélange units have so far considered that their deformation is contemporaneous with their burial (Ikesawa et al., 2005; Ikesawa et al., 2003; Kimura and Mukai, 1991; Onishi and Kimura, 1995; Ujiie, 1997; Ujiie et al., 2007), which implicitly discards a possible influence of the Miocene collision, much more recent than subduction processes. This issue is in fact not so easy to solve, as the tectonic influence of the collision is attested on units from the Shimanto Belt located south of the mélange units considered here (Raimbourg et al., 2017). In addition, ages of deformation obtained in pseudotachylytes from faults bounding the Mugi (Tonai et al., 2016) or the Kure (Honda et al., 2011) mélange support post-subduction activity, possibly related to the collision.

The main argument in favor of simultaneous mélange internal deformation and subduction is the fact that this deformation is almost absent in nearby coherent units. This very strong contrast in deformation style and intensity between mélange units and adjacent coherent units suggests that mélange internal deformation was acquired relatively early in its history, at least before mélange units were stacked upon adjacent coherent units. In contrast, the Miocene collisional event (Charvet, 2013) should have affected the whole tectonic pile made of mélange units sandwiched between coherent units. On the other hand, the very localized deformation between units, in particular the occurrence of “out-of-sequence” thrusts, such as the NTL (Kondo et al., 2005) or the fault network cutting across Kure mélange and adjacent units (Mukoyoshi et al., 2006), could well be the expression, at least to some extent, of posterior later collision phase. The amplitude of this collisional phase is unclear, as there is no remaining exposed evidence of the colliding microblock. For these reasons, in the following section, we consider that all deformation distributed within the mélange is coeval with subduction, while the timing of faulting, either during subduction or during later collision, is unclear.

4 Deformation within mélanges in the study area

4.1 Structures of distributed deformation

Distributed deformation is illustrated by the presence of a pervasive foliation (S1) in the pelitic matrix, carrying flattened sandstone lenses. The foliation in Hyuga mélange strikes NE-SW and has a low dip to the NW, e.g. N044°E 40NW in site 112 or N065°E 33NW in site 202 (Figure 4). In Okitsu mélange, the foliation strikes WNW and is close to the vertical, e.g. N064°E 87NW in site 220 (Figure 5). In Mugi mélange, the foliation strikes WNW and is close to the vertical, e.g. N076°E 81NW at sites 346-347-348, or N050°E 89NW at site 349 (Figure 6)

Lineation is generally difficult to observe on the foliation, except in the Hyuga mélange, which has recorded the highest temperature conditions during deformation in its eastern area (Table 1). There, lineation trends NW-SE, e.g. N140-N150°E on cross-section A-B, or N134°E on cross-section C-D (Figure 4).

Macroscopic deformation is mainly represented by abundant cracks filled with quartz within sandstone lenses, especially in the necked domains towards the tips of the sandstone lenses (Figure 7-A). Another conspicuous deformation feature within the mélange is a network of shear bands (Figure 7, Figure 8 and Figure 9) deflecting the foliation within the shale matrix and the sandstone lenses. Shear bands often occur in zones of high concentration of quartz-filled cracks (Figure 7A). The spacing between adjacent shear bands is variable, from ~1m to a few cm (see below). Some shear bands contains synkinematic lenses of precipitated quartz (Figure 7B and Figure 8) while in other cases shear bands are not mineralized (Figure 7A).

4.2 Microstructures of distributed deformation

The patterns of deformation observed at outcrop-scale are transposable to smaller scales. Small lenses composed of sandstones or siltstone, but also of precipitated quartz forming elongated boudins within the foliation, are embedded within the shale matrix. These lenses are truncated by a

dense array of quartz-filled fractures perpendicular both to the foliation and to the lineation, i.e. parallel to the YZ plane (Figure 10). All the elongated and truncated lenses, including the ones formed by precipitated quartz, are deflected by shear bands (Figure 11, Figure 12, Figure 13). This deflection provides a cross-cutting criterion of anteriority of veins relative to shear bands. Quartz lenses are most often continuous across shear bands (Figure 11 and Figure 12), even if sometimes their thickness is much reduced by local high strain (see the necking structures in the central part of Figure 11 and Figure 12).

At the mineral scale, the shear bands have a composite structure, incorporating a network of chlorite-filled shear zones (Figure 13A) in addition to elongated domains of precipitated quartz (Figure 13B). In the latter quartz domains, abundant healed microcracks, materialized by secondary fluid inclusion planes, are oriented perpendicular to the local stretching direction (Figure 13B).

4.3. Structures of localized deformation

As mélange faults have already been largely studied (Kitamura et al., 2005; Kondo et al., 2005; Sakaguchi, 2003; Ujiie et al., 2007, Mukoyoshi et al., 2009), this section only briefly summarize their characteristics relevant for the present study. In contrast to distributed deformation structures, localized fault are not scale independent: they represent large-scale structures on the outcrops, always > 10m in length and with an overall thickness of 0.1 – 10m. In Hyuga, Mugi and Okitsu mélanges, the largest fault zones constitute the northern boundaries of the whole mélanges. The NTL, forming the northern boundary of the Hyuga mélange, is a major fault of the belt, associated with a large gap in the distribution of biostratigraphic ages (Hara and Kimura, 2008) and in paleotemperatures ($\Delta T°$ ~100°C; (Raimbourg et al., 2014a; Raimbourg et al., 2017)). In contrast, in Okitsu and in Kure areas there is no biostratigraphic age gap between the mélange matrix and the coherent formation north of them (Kiminami et al., 1992; Taira et al., 1988) while the paleotemperature gap is small in Okitsu (~30°C, vitrinite reflectance data from Sakaguchi (1999b)

using conversion factors from Sweeney and Burnham (1990)), and absent in Mugi (Kitamura et al., 2005).

In some instances, fault zones also form the boundaries between individual thrust sheets within the mélange unit (Figures 5 and 6). In particular, the Mizoochi fault zone that separates the upper and lower sections of Mugi mélange, is associated with a temperature gap of 60°C (Kitamura et al., 2005). Strain is very heterogeneous within fault zones, and one or several cm- to dm-thick layers of cataclasites or ultracataclasites are present. The microstructure of the cataclasites and ultracataclasites is much different from the mélange, as it is composed of rounded clasts of variable sizes embedded in a very fine-grained, dark matrix. In the case of Mugi and Okitsu, evidence of melting is found within the ultrafine-grained layers, considered therefore as pseudotachylytes (Ikesawa et al., 2005; Ikesawa et al., 2003; Kitamura et al., 2005; Sakaguchi, 2003). A noteworthy feature of fault zones is the quasi-absence of quartz precipitation. Localized deformation structures rework or cut quartz veins of all kinds, and are therefore posterior to distributed deformation structures.

4.4 Deformation kinematics

The kinematics of distributed deformation structures shares common features in all the studied mélange units (Figure 4, Figure 5, Figure 6). First, macroscopic quartz-filled crack veins in boudins are consistently perpendicular to the foliation plane for the three mélanges (Figure 10). In the case of the Hyuga mélange for which a lineation is observable, quartz-filled cracks are oriented N006°E on average, i.e. nearly perpendicular to the average direction of transport (N134°E). Second, kinematics of shear bands and ductile-brittle structures correspond to a top-to-the-SE sense of shear, with slickenlines oriented N134 – N150°E, in the Hyuga mélange, N145 – N157°E in the Okitsu mélange, and N157 – N166°E in the Mugi mélange. This top-to-the-SE sense of shear is consistent with the overall convergence direction in the whole Shimanto Belt and the asymmetry of the subduction zone. Third, the shear bands have a lower averaged dip than the mélange foliation, both in cases where

mélange foliation is steeply (Okitsu and Mugi) or gently (Hyuga) dipping. Finally, the slickenlines of the major pseudotachylyte-bearing faults, observable at the boundary of the Okitsu and Mugi mélanges, are oriented N018°E and N070°E on average in the former and latter case, respectively. The kinematics of these faults is thus not compatible with the NW-SE direction of motion observed in mélange shear zones.

5-Discussion

5.1 Structures and microstructures of distributed deformation in mélanges

Foliation-parallel veins are a conspicuous feature of tectonic mélanges in the Shimanto Belt as shown on Figures 9 to 13. The orientation of healed microcracks (Figure 13B) and the crystallographic-preferred orientation of quartz shows that these veins grew through successive events of fracturing perpendicular to the stretching direction (Palazzin et al., 2016). Quartz-filled cracks in sandstone lenses, perpendicular to foliation, and veins parallel to the foliation (Figure 10 to Figure 12) are therefore kinematically consistent and were formed contemporaneously in spite of their different orientation. Foliation-parallel veins have also been reported in the Franciscan Complex in the USA, in the Kodiak Complex in Alaska, in the Chrystalls Beach Complex in New Zealand, and in the Internal Ligurian Units in Italy (Fagereng and Harris, 2014; Fagereng et al., 2011; Meneghini et al., 2009; Mittempergher et al., 2018). In these examples as well as in Shimanto, foliation-parallel veins are interpreted as extensional shear veins and record increments of deformation in crack-seal textures (Fagereng and Harris, 2014; Fagereng et al., 2011; Fisher and Byrne, 1990; Fisher and Brantley, 1992, 2014; Fisher et al., 1995). Conditions of formation of such veins span a large temperature range. They can be found at low temperatures (~150°C) in the Mugi mélange lower and “colder” thrust sheets (Kitamura et al., 2005), in the relatively shallow subduction channel of the Apennines (Mittempergher et al., 2018; Vannucchi et al., 2010), in unlithified to semi-lithified rocks from the Internal Ligurian Unit (Meneghini et al., 2007) and during the very shallow (40-70°C) stage of burial of Infra-Helvetic Flysch units of the Alps (Dielforder et al., 2015). Nevertheless, veins were also formed

at higher temperatures (250-300°C) in the Hyuga Tectonic mélange (Palazzin et al., 2016; Raimbourg et al., 2015), in the Otago Schists (Fagereng and Harris, 2014) or in Kodiak (Vrolijk et al., 1988) (see also the compilation of temperatures in (Raimbourg et al., 2018)). Additionally, at thin section scale, a network of microscale shear bands, forming a anastomosed network parallel to the foliation, contain a large proportion of preferentially-oriented chlorite flakes (Figure 13A), as was reported on other mélange examples (e.g. Meneghini et al. (2009)). Bulk-rock deformation at depth, for temperature conditions in the range ~150-300°C, is therefore the result of combined microfracturing, solution precipitation of quartz and slip on chlorite plates.

The other conspicuous deformation feature we observed in the different mélanges of the Shimanto Belt are macroscopic shear bands (Figure 7 to Figure 9) at a low angle to the foliation. Shear bands of similar geometry are also present in many tectonic mélanges, such as in Kodiak (Fisher and Byrne, 1987), or in the subduction channel exposed in the Northern Alps (Bachmann et al., 2009), for T that range from 150-400°C. There, deformation involves a combination of distributed shear zones and extension fractures (mainly oriented parallel to the foliation), which an increasing abundance with depth along the subduction channel.

The chronology of the deformation structures is similar between Okitsu, Mugi and Hyuga mélange zones. The first stage of deformation involves layer-parallel extension, which results in the development of necking of sandstone lenses, formation of tension cracks perpendicular to foliation and foliation parallel veins (which themselves are to a large extent the result of repeated tension microcracking, Figure 13B and Palazzin et al. (2016)). The elongated and fractured sandstones lenses and foliation-parallel veins are then deflected by macro- (Figure 7 to Figure 9) and microshear zones (Figure 11 to Figure 13), developed in a second stage.

A further indication on the relative timing of microstructures with respect to the mélange tectonic evolution is provided by the comparison between Mugi, Okitsu and Hyuga, which experienced increasing peak-T conditions. Only in the western domain of Hyuga, where the metamorphic

363 temperatures were the highest (ca. 240-270°C), a clear mineral lineation is visible, suggesting that
364 lineation developed for maximum temperature conditions. The direction of motion indicated by the
365 slickenlines over ductile-brittle structures carried by shear zone planes is parallel to the lineation
366 (Figure 4), which shows that the shear bands themselves were active for the highest T conditions, at
367 peak-burial conditions. Furthermore, in the Hyuga mélange, poles to tension veins (N096) and
368 direction of slip on shear bands (N134) are close to each other in orientation, which suggests that
369 veins and shear bands developed during the same framework of burial, but probably at different
370 depths.

371 **5.2 Kinematics of mélange deformation**

372 The foliation is well-developed in the three mélange units studied here, whereas the lineation is well-
373 defined only in the western domain of the Hyuga Tectonic mélange (Figure 4, see also Raimbourg et
374 al. (2014a)). In the rest of mélange exposures (eastern part of Hyuga, Okitsu and Mugi areas), where
375 temperatures did not exceed 240°C, it is therefore unclear whether the sandstone lenses within the
376 foliation formed by flattening, pure or simple shear.

377 This evolution of finite strain markers with temperature is further supported by anisotropy of
378 magnetic susceptibility (AMS) data. Sandstone lenses from the two sections of Mugi mélange shows
379 a magnetic fabrics corresponding to a flattening régime (Kitamura and Kimura, 2012), with a well-
380 defined foliation and magnetic lineations scattered in the magnetic foliation plane. In contrast, at
381 higher temperatures (~340°C, i.e. Palazzin et al. (2016)) within the Makimine mélange, the magnetic
382 fabrics change towards a 3-dimensional shape of a L-S tectonite (Kitamura and Kimura, 2012) and the
383 magnetic lineations are clustered around NNW-SSE direction, parallel to the stretching lineation
384 (Raimbourg et al., 2014a). The same magnetic fabrics was described in Okinawa islands, also
385 belonging to the Shimanto Belt, in an underplated mélange unit (Ujiie et al., 2000). In tandem with
386 the AMS fabrics, analysis of the 3D shape of radiolarians in the higher-grade units of the Shimanto

Belt (T~350°C) has also revealed a preferred elongation direction, parallel to the shear direction (Kimura and Mukai, 1991; Toriumi and Teruya, 1988).

Extension parallel to the underthrusting direction is therefore revealed by the development of a clear stretching lineation, by the AMS or by the shape fabrics of radiolarians in the higher-temperature examples of mélanges, while in the lower temperature example the strain ellipsoid is more ambiguous, partly because of a lack of reliable strain markers.

In addition, in the examples treated here, the clearest microstructures, in terms of kinematics, are the macroscopic shear bands that develop within the mélanges, with directions oriented NW-SE in Hyuga and NNE-SSW in Okitsu and Mugi mélanges. These shear bands indicate consistently top-to-the-SE shear deformation in any example. This sense of shear is consistent with burial and underthrusting of the mélange below Eurasia in Early Cenozoic times (Raimbourg et al., 2014a; Sakaguchi, 1999b). Furthermore, as shear band dip is lower than the main foliation (Figure 4 to Figure 6), when the latter is restored back to underthrusting attitude (i.e. with a low landward dip), the shear bands become extensional structures.

Similar to these Shimanto case studies, the most commonly reported kinematic indicator in worldwide examples of mélange reflect layer parallel coaxial extension, top-to-the-trench shearing or both. In most cases, kinematics are interpreted as the result of shear along or near a master décollement (Byrne and Fisher, 1990; Fisher and Byrne, 1987, 1990). In the Uyak Complex in Alaska, conjugate normal faults are reported, with the set of normal faults synthetic with subduction-related shear dominant over the other one (Byrne and Fisher, 1990). In the Marin Headlands of the Franciscan Complex (Meneghini and Moore, 2007) or in the Mugi mélange of the Shimanto Belt (Kitamura and Kimura, 2012), structures are interpreted in terms of Y-P-R brittle fabrics and the abundant R planes are similar, geometrically and kinematically, to the extensional shear bands described in our work. In the northern Apennines, extensional shear bands and faults are also reported, but two conjugate sets seem to be present (Vannucchi et al., 2010). In the subduction

channel in the Northern Alps, shear bands are widely distributed, some of them with S-C geometry, and the preferred sense of shear is synthetic with the master shear on the décollement during subduction (Ring et al., 1989). Therefore the general pattern is that extensional shear bands, sometimes conjugate but in most cases synthetic with underthrusting-related shear, dominate the deformation in mélanges.

5.3 Underplating process of mélange

Mélange units in the Shimanto Belt have a relatively constant structure, with the imbrication of individual sheets composed of a basaltic sole below a thicker sequence of tectonic mélange composed of sedimentary material (and minor occurrences of other ocean-floor lithologies such as radiolarites or red and black shales). In addition, some of the basalt lenses or layers are associated with fault zones, for example in the Mugi (Ikesawa et al., 2005; Kitamura et al., 2005) or Okitsu mélanges (Ikesawa et al., 2003; Sakaguchi, 2003; Sakaguchi et al., 2006). The imbricated structure and the presence of faults has led to the model of localized underplating (Figure *14*B), to account for the stacking of mélange sheets to the upper plate (Fisher and Byrne, 1990; Ikesawa et al., 2005; Kimura and Mukai, 1991; Onishi et al., 2001; Sample and Fisher, 1986). In this model, each individual thrust sheet is underplated at the base of the overlying plate as a result of the stepdown of the décollement to the upper levels of the basalt of the subducting plate. The resulting structure, after successive events of décollement step-down, is a stack of imbricated thrust sheets.

Such a model of imbrication during underplating share many similarities with fold-and-thrust belts, which have been widely studied in the external domains of collisional orogens (Bally et al., 1966; Chapple, 1978). Kinematics of deformation in fold-and-thrust belts has for example been derived from passive strain markers (e.g. oolites) in the Northern Mountains, in the Appalachians, showing that within thrust sheets the shortening axis of finite strain is close to the parallel to the transport direction (Evans and Dunne, 1991). Microtectonic analysis, applied to fold-and-thrust belts, has shown similarly that meter-scale faults record the same pattern of horizontal shortening as can be

437 deduced from imbrication of thrust sheets over a main thrust, as for example in Taiwan (Angelier et
438 al., 1986; Angelier et al., 1990; Barrier and Angelier, 1986; Chang et al., 2000) or the French Jura Belt
439 (Homberg et al., 2002).

440 Accordingly, even if most of the strain is localized on a master fault, the model of localized
441 underplating (Figure *14*B) involves evidence for contractional deformation within the stacked thrust
442 sheets. Contractional deformation has indeed been described in some mélange examples. For
443 instance, deformation within the Kodiak mélange is divided into two stages, D1 related to shearing
444 during burial, D2 related to fold and thrusting and to the formation of a slaty cleavage, during
445 underplating and imbrication (Fisher and Byrne, 1990; Sample and Fisher, 1986; Sample and Moore,
446 1987). Contraction during underplating is also described in the mélange along Akamatsu river in
447 eastern Shikoku, Japan (Kimura and Mukai, 1991). Similarly, although the subduction channel in the
448 Alps is restricted to relatively shallow depths and temperatures (below ~150°C), early extensional
449 structures are overprinted by compressional structures (Vannucchi et al., 2008).

450 A major ambiguity still regards the timing of the folds and thrusts that characterize the contractional
451 deformation recorded in accretionary prisms such as Kodiak or the Shimanto Belt. Instead of having
452 formed during underplating, it may as well result from a posterior stage of deformation, within the
453 accretionary wedge itself. In the Shimanto Belt, a large-scale collision stage has been described,
454 which has largely reworked the whole structure and may correspond to most or all mesoscale
455 contractional structures (Charvet, 2013; Charvet and Fabbri, 1987; Raimbourg et al., 2017).
456 Furthermore, the first-order faults, such as the Nobeoka Tectonic Line (Kondo et al., 2005), are out-
457 of-sequence features, formed within the wedge after accretion. In the Alaskan case, the transition
458 between underplating and later-stage intra-wedge shortening is rather unclear. As a consequence, it
459 is difficult to assign contractional deformation unambiguously to underplating.

460 Furthermore, contractional deformation structures recorded in the three mélange zones investigated
461 here are an uncommon feature and most of the deformation results from shear and non-coaxial

462 extension. In the other examples from the Shimanto Belt, distributed shortening is either limited to
463 the vicinity of large-scale faults (Kimura and Mukai, 1991) or not observed (Hashimoto and Kimura,
464 1999).

465 A consistent model of mélange underplating should therefore incorporate both the repetitive
466 formation of faults to stack thrust sheets one upon another and the dominance of extensional
467 deformation distributed in the volume of mélange units. Rather than a succession of two stages, a
468 possible model could consider that extension recorded in shear bands actually results from, and not
469 predates underplating (Figure *14*A).

470 Let us assume that, as an initial stage, mélange absorbs all, or a large fraction, of the relative
471 displacement between the subducting and overriding plates. Such an assumption is closely related to
472 the "subduction channel" model, where viscous deformation is broadly distributed within a channel
473 of several hundreds of meters of thickness, composed of the incoming sedimentary sequence (or a
474 fraction of it) between two rigid walls (Cloos, 1982; Cloos and Shreve, 1988a, 1988b; England and
475 Holland, 1979; Mancktelow, 1995; Raimbourg et al., 2007b; Shreve and Cloos, 1986; Vannucchi et al.,
476 2012b). The material flowing within the channel is neither part of the lower or upper plate; its
477 velocity varies between null on top and plate convergence rate at the bottom of the channel (in
478 upper plate reference frame). This kinematic role of mélange is suggested by the abundance of
479 deformation microstructures (tension cracks, network of shear zones at all scales, stretching
480 lineation, shape of rigid lenses), even if no strain markers enables to evaluate the absolute strain. In
481 addition, the subduction channel model also postulates that there is no major, actively deforming
482 fault bounding the sediment-filled channel. This point, discussed in the following section, is
483 supported by the fact that the faults that limit the mélange in its present geometry were not active
484 contemporaneously.

485 It is likely that at some point, shear will become more easily accommodated within a localized fault
486 through the subducting basalts than within the sediment pile, for example because of strain- or

metamorphic-hardening. This scenario is required to form the internal architecture of mélange units, with a stack of several basalt-soled sheets (Figure 5 and Figure 6). After formation of such a fault within the oceanic crust, further subduction of the deforming mélange, connected to a more localized slip zone within the basalts, results in thinning the subducting sediment pile. This is readily apparent when comparing the velocity profiles across several sections at different depths. In the model, conservation of material is imperative. Therefore, if the channel walls are fixed, the flux through any section of the channel must be equal. Conversely, if the fluxes vary along the channel length, then motion of the walls are required. Conservation of the material implies therefore that when the deforming zone is thinner than incoming thickness, the roof boundary of the "channel" is necessarily pushed upwards, to accommodate a larger influx of material than what is flowing in (Figure 14A'4). As a result, the "nose" of the channel gets longer (at a velocity equal to burial) and its opening angle gets smaller with time (Figure 14A2 to A'4). The material flowing through it accommodates this thinning by the formation of synthetic extensional shear zones. Eventually, as the shear strain rate increases towards the tip of the channel (because the material is flowing in a thinner channel), at some point a new fault forms within the underlying basalts, and a new thrust sheet starts forming.

Unlike models of "localized" underplating, where material is strong and deformation is localized on faults, such a model of "distributed" underplating considers the mélange as soft and deformable, thus accommodating most of underplating-related strain. One of the advantages of this model is to account for the lack of shortening deformation within mélange units and the concomitance of extension and underplating, in contrast to the examples of fold-and-thrust belts cited above. This model also enables the connection between mélange deformation (distributed within the whole subducting pile) and fault formation during underplating, while localized models of underplating consider that slip occurs principally on the décollement (Fisher and Byrne, 1990; Ikesawa et al., 2005; Kimura and Mukai, 1991; Onishi et al., 2001; Sample and Fisher, 1986), which is equivalent to completely disregarding, in terms of strain accommodation, mélange distributed deformation. Finally,

513 our model also accounts for the thinning of the sedimentary pile (geometrically necessary because of
514 the distributed extensional shear bands), which is not incorporated in other underplating models.

515 **5.4 Model of subduction plate boundary**

516 *5.4.1 Relationship between localized and distributed deformation*

517 Evidence of adjacent brittle deformation features, including pseudotachylyes (Ikesawa et al., 2003;
518 Kitamura et al., 2005; Meneghini et al., 2010; Rowe et al., 2011; Rowe et al., 2005; Rowe et al., 2013)
519 and distributed deformation in mélanges has led to a model of plate interface incorporating
520 simultaneously zones of highly localized slip and domains of more distributed slip (Rowe et al., 2013).
521 This generic fault zone, forming the plate boundary, follows the fault zone model by (Faulkner et al.,
522 2010; Faulkner et al., 2003) composed of a ~100m-1km-wide "damage" zone, ~1-5m-wide fault-core
523 and ~mm-to-cm-thick slip zones.

524 The coexistence, of distributed deformation and localized slip features, such as pseudotachylytes, in
525 Kure (Mukoyoshi et al., 2006), Okitsu (Sakaguchi, 2003; Sakaguchi et al., 2006), Mugi (Ikesawa et al.,
526 2005) or Hyuga (Kondo et al., 2005) mélange areas within the Shimanto Belt, might suggest that they
527 were active at the same time, but our closer examination rather showed that they appear
528 disconnected for different aspects.

529 Disconnection is in some cases geometrical, i.e. fault zones and pseudotachylytes are late-stage, or
530 "out-of-sequence" faults, cutting across tectonic contacts and distributed deformation formed during
531 underthrusting. For example, the faults zones (including pseudotachylyte-bearing faults) present in
532 the Kure mélange (Mukoyoshi et al., 2006) cut across the boundary between the mélange and the
533 adjacent tectonic unit, so these faults were formed after the deformation within the mélange
534 acquired during underthrusting. This two-staged evolution is confirmed by age constraints: although
535 underthrusting age is imprecise, the Kure mélange is associated with the Cretaceous Belt (Taira et al.,
536 1988). In contrast, radiometric ages on the pseudotachylyte yield much younger ages of ca. 18Ma

(Honda et al., 2011), which were interpreted as reflecting a post-subduction stage of collision in Early Miocene (Raimbourg et al., 2017). Similarly, the pseudotachylyte-bearing ultracataclasite forming the roof thrust of the Mugi mélange was dated by K-Ar radiochronology at ~23-29Ma, while authigenic illite formed synchronously with burial and deformation within the mélange yielded ages between 85 and 48Ma (Tonai et al., 2016). In Okitsu, the maximum paleotemperature, revealed by the vitrinite reflectance geothermometer, is higher in the mélange by ~30-50°C than in the overlying unit (Sakaguchi, 1999b; Sakaguchi et al., 2006). As discussed in (Ujiie et al., 2007), the boundary thrust, including the pseudotachylyte-bearing fault, is therefore interpreted as an out-of-sequence thrust, cutting across the thermal structure inherited from subduction/underthrusting stage. Similarly, the large-scale tectonic structure of the Cenozoic Shimanto Belt on Kyushu shows that the large-scale fault NTL is a late-stage feature cutting across a number of tectonic units and their internal deformation, including the Hyuga Tectonic mélange (HTM) (Murata, 1996, 1997, 1998; Raimbourg et al., 2014a). The NTL constitutes the roof thrust of the HTM on the eastern coast, but further west the NTL cuts across the basal boundary of the HTM, so that the footwall of the NTL is there composed of the coherent turbiditic formation underlying the HTM (Figure *2*). Therefore, while on the eastern coast the mélange deformation was interpreted as damage resulting from slip on the NTL (Kondo et al., 2005), the map-scale relationships between the tectonic mélange and the NTL show that in general mélange deformation predates the fault slip event on the NTL.

In these examples, the mélange deformation within the thrust sheets, interpreted as related to underthrusting, predates more localized deformation on faults, associated in most cases with a distinct, later-stage event. In the classical model of mélange underplating (Fisher and Byrne, 1990; Ikesawa et al., 2005; Kimura and Mukai, 1991; Onishi et al., 2001; Sample and Fisher, 1986) (Figure 14B), there is also a clear disconnection between the mélange-forming deformation, during burial, and slip on thrust sheets-bounding faults, during underplating. In the alternative model we propose in Figure *14*A, distributed deformation in the mélange during underplating, and repeated events of slips on faults within basalts, are coeval, although they occur at different locations along dip. But

563 irrespective of the model of underplating, there is no configuration such as proposed in Rowe et al.
564 (2013) where large-scale faults and distributed slip act in parallel. Furthermore, as for the different
565 examples from the Shimanto Belt, in most instances the most localized features, pseudotachylytes,
566 are a later-stage event occurring within the wedge, after the underplating of the mélange at depth.

567 *5.4.2 Seismic vs. aseismic slip along the interface – rheological models*

568 A cm- or dm-thick fault zone deforming discontinuously through repeated earthquakes, or a
569 ~hundreds of meters-thick subduction channel deforming through distributed shear, constitute two
570 theoretical end-members of the plate interface (Fagereng and Sibson, 2010). Tectonic mélanges, in
571 as much as they correspond to fossil plate interfaces, are thick deforming zones akin to the second
572 endmember, and their role in aseismic slip, occurring in non-coupled portions of the plate
573 interface(e.g. (Loveless and Meade, 2010; Moreno et al., 2010)), has long been hypothetized
574 (Fagereng and Sibson, 2010).

575 Nonetheless, the actual rheology of tectonic mélanges is complex, as a result of their heterogeneous
576 composition, and the distribution of strain and strain rate may depend on the proportion of the rigid
577 blocks within the more deformable matrix (Fagereng and Sibson, 2010). Furthermore, the stability of
578 mélange deformation, hence their potential to host large earthquake, might also depend on the
579 strain rate applied, as suggested by friction tests on clay+quartz mixtures (den Hartog et al., 2012;
580 Den Hartog and Spiers, 2014): subduction channels deforming by velocity-strengthening processes
581 way switch to velocity-weakening behavior and instable slip upon an increase in strain rate (Fagereng
582 and Den Hartog, 2017).

583 To account for mélange rheology, microphysical models developed from deformation experiments of
584 a mixture of quartz grains embedded in a phyllosilicate matrix, are particularly appropriate (den
585 Hartog et al., 2013; Den Hartog and Spiers, 2014; Niemeijer, 2018; Niemeijer and Spiers, 2007;
586 Niemeijer et al., 2008). Bulk strain results from the contribution of quartz grain deforming by
587 pressure-solution, and frictional slip on a phyllosilicate foliation. Unlike classical rate-and-state

588 friction laws with parameters a and b (Dieterich, 1994; Ruina, 1983), geometrical parameters such as
589 shear zone thickness can be explicitly considered in microphysical models and their effect on slip
590 stability considered (e.g. (Fagereng and Den Hartog, 2017)). The few observations developed here on
591 tectonic mélange structures and microstructures of deformation provide direct constraints on such
592 microphysical models, hence on the rheology of the shear zones constituting the plate interface.

593 A key aspect of the microphysical models, necessary to trigger velocity-weakening behavior, is the
594 competition between slip-induced dilatational strain and compaction resulting from thermally
595 activated deformation of the rigid clasts. Stress corrosion cracking, i.e. sub-critical crack growth in
596 quartz, is invoked as a major process in the deformation of the rigid quartz clasts (den Hartog et al.,
597 2012; Den Hartog and Spiers, 2013), on the basis of observations in sandstone compaction
598 experiments (Schutjens, 1991). Nonetheless, because of the lack of quantitative constraints,
599 microcracking is not incorporated in the physical formulation of the clast deformation, which is
600 described solely in terms of pressure solution.

601 The structures and microstructures shown in this work point indeed to the major role played by
602 fracturing in the deformation of the rigid bodies at all scales. As shown by the example of the Mugi
603 mélange (Figure 10B and Hashimoto et al. (2006)), tension veins in boudin necks start forming at
604 shallow conditions, for T as low as ~150°C, marking the transition from soft sediment behavior to the
605 brittle behavior of cemented, low-porosity rocks (Fagereng et al., 2018). Pervasive fracturing of
606 competent bodies, from meter-scale lenses of sand- or siltstones to millimeter-scale veins of quartz,
607 can be found over the whole seismogenic depth range down to the transition to plastic deformation
608 (Figure 10 and (Palazzin et al., 2018)). Multiple events of microfracturing of quartz veins, attested by
609 crack-seal microstructures (Fisher and Byrne, 1990; Fisher and Brantley, 1992, 2014; Ujiie et al.,
610 2018) or quartz textures revealed by cathodoluminescence (Raimbourg et al., 2018; Raimbourg et al.,
611 2015) also suggest that fracturing is active throughout burial. The size and spacing of the rigid objects
612 deforming through cracking provide characteristic transport distances for pressure-solution, even in

613 the absence of the physical laws for cracking itself. Assuming that silica, the vein-forming material, is
614 dissolved and precipitated locally, then the spacing between fractured quartz veins or silt-/sandstone
615 clasts gives an estimate of the transport distance, a key parameter of the pressure-solution flow laws
616 (Gratier et al., 2009). In the most strongly deformed areas, pervasive veining (Figure 11 and Figure
617 12) form foliation-parallel lenses of quartz with a spacing of the order or below 1mm (Palazzin et al.,
618 2016). Bulk-rheology, relevant at the plate tectonics scale, should account for imbricated scales,
619 including the deformation of rigid grains in a phyllosilicate matrix explicitly considered in the
620 microphysical models (Den Hartog and Spiers, 2014; Niemeijer and Spiers, 2007; Niemeijer et al.,
621 2008), but also larger scales, in particular the behavior of rigid lenses (in particular of precipitated
622 veins) in a quartz+phyllosilicate matrix.

623 Additionally, the large density of mode I cracks accompanying deformation of all rigid bodies (Figures
624 7 to 13) is a clear evidence of high fluid pore pressure attending deformation (Byrne and Fisher,
625 1990), even if the determination of in-situ fluid pressure from fluid inclusion record has remained so
626 far elusive (see the review in (Raimbourg et al., 2018)). This bears some influence on the
627 clasts+phyllosilicate microphysical model, as dilatancy, by decreasing the pore fluid pressure and
628 decreasing the effective stress, has a strengthening effect on slip (Segall and Rice, 1995). Variations in
629 fluid pressure have for example been described in Kodiak mélange (Vrojlik, 1987) or in the Shimanto
630 Belt (Raimbourg et al., 2014b), showing that the retroaction between fluid pressure and slip should
631 be explicitly considered.

632 The last insight provided by the natural examples shown in here regards the nature of the
633 phyllosilicate forming the network of shear zones, which is principally chlorite throughout the
634 temperature range (Figure 13A). A similar development of a network of chlorite is also reported in
635 Kodiak (Fisher and Byrne, 1987) and in the Franciscan Complex (Meneghini et al., 2009). In contrast,
636 most friction experiments used to infer plate boundary rheology are based on mixtures of smectite,
637 illite and quartz (Ikari et al., 2007; Saffer et al., 2001; Saffer et al., 2012; Saffer and Marone, 2003).

Friction experiments on chlorite show no large difference between illite and chlorite in terms of friction coefficient (Ikari et al., 2009; Moore and Lockner, 2004). Nevertheless, permeability differ significantly, and chlorite gouge have two to three orders of magnitude higher permeability than illite gouges (Ikari et al., 2009), which potentially plays a role when considering dilatation and pore pressure changes during slip. Furthermore, systematic data about dependence of friction on temperature, available for quartz+illite/muscovite mixtures (den Hartog et al., 2012, 2013; Den Hartog and Spiers, 2013) or smectite-rich natural sediments (Sawai et al., 2017), are still lacking for chlorite.

6-Conclusions

The comparative study of several tectonic mélange units within the Shimanto Belt revealed common features, providing insights into the processes occurring along the subduction plate boundary at depth. Several conclusions can be drawn from mélange micro- and macrostructures of deformation, regarding the processes of underplating and the distributed vs. localized character of deformation:

1) Distributed deformation, at the origin of the development of block-in-matrix structure of the mélanges, results from slip on a pervasive network of shear bands, ranging from meter-scale, quartz-filled structures to microscopic, chlorite-filled ones. Deformation on shear bands is accompanied by pervasive veining, either in cracks formed perpendicular to extension in more competent sandstone or quartz lenses, or in extension veins parallel to the foliation.

2) Kinematics of deformation, as deduced from the slip on shear bands, is a consistent top-to-the-trench shear. As shear bands have in average a lower dip than the foliation, they are interpreted as extensional structures.

3) Underplating is required by the repetition of several mélange thrust sheet units. Nonetheless, the absence of contractional structures within the mélange leads to a new model, where distributed extension within the mélange occurs during underplating. This model of “distributed” underplating,

662 constrasting with “localized” underplating models, is in accordance with the strong partitioning of
663 strain within the mélange material.

664 4) Localized deformation on faults, including pseudotachylytes, occurs in many instances *after*
665 underplating, as intra-wedge deformation, while mélange internal deformation occurs *before* (i.e.
666 underthrusting) and *during* underplating. There is no evidence for a preserved structure of the plate
667 boundary comprising a roof thrust and underlying mélange deforming simultaneously.

668 5) Mélange distributed deformation is a candidate for the aseismic slip observed along certain
669 portions of active subduction plate interfaces. Mélange deformation features that should be
670 incorporated into models of the plate rheology (such as microphysical models by Den Hartog and
671 Spiers (2014)) include (i) the role of fracturing for clasts/rigid bodies deformation, (ii) the variable size
672 (hence deformation processes) of the rigid bodies embedded in a weaker matrix, (iii) the large fluid
673 pressure accompanying deformation and (iv) the role of chlorite to form the micro-scale network of
674 shear zones within the weak matrix.

675

676

677

678 # Acknowledgements

679 This work has received funding from (i) the European Research Council (ERC) under the seventh
680 Framework Programme of the European Union (ERC Advanced Grant, grant agreement No 290864,
681 RHEOLITH), (ii) the Labex VOLTAIRE (ANR-10-LABX-100-01) and (iii) the program “Sakura” by the
682 French Ministry of Foreign Affairs. We thank the Editor and the two anonymous reviewers for their
683 constructive comments on an earlier version of the manuscript.

684

Figure and Table captions

Figure 1: Tectonic setting of the Shimanto Belt, along the southern border of Japan (Kimura et al., 2016). The studied mélange units are located on Kyushu (see Figure 2) and Shikoku islands (see Figure 3).

Figure 2: Geological map of Shimanto Belt on eastern Kyushu. The Hyuga mélange unit is located below the Nobeoka Tectonic Line (NTL) over most of the area, except for the northeastern area, where the NTL cuts across the limit between “Coherent Hyuga” and “Hyuga Tectonic mélange” (enlarged rectangle at upper right). The Hyuga mélange incorporates, in addition to strongly sheared sedimentary rocks, sheets of basalt and to a lesser extent of red shales. Adapted from Murata (1997). Cross-sections A-B and C-D in Figure 4.

Figure 3: Distribution of mélange units within the Shimanto Belt on Shikoku, adapted from Taira et al. (1988).

Figure 4: Kinematics of deformation within the Hyuga mélange (light blue color in the map and stereoplots). Stereo diagrams are equal area, lower hemisphere, with the numbering underneath referring to outcrops. Foliation is shown as the red plane, while planes with arrows correspond to shear bands. Cross-section locations refer to Figure 2.

Figure 5: Structures and kinematics of deformation in the Okitsu mélange unit.(A) Map of Okitsu area, with stereoplots of deformation kinematics. In blue stereoplots, compiling data from mélange structures, foliation is shown as the red plane, while planes with arrows correspond to shear bands. The pseudotachylyte-bearing fault zone along its northern boundary is associated with a top-to-the-SSW thrust motion. Abundant shear zones in the mélange indicate top to the SE thrusting. Kinematic data on fault zone from Sakaguchi (2003). The average azimuth of slicken lines is shown as the thick black ticks. Stereo diagrams are equal area, lower hemisphere. (B) Cross-section of the stack of units constituting the Okitsu mélange, along the profiles X-X’, Y-Y’, Z-Z’ in (A). Basalt is present in thick

709 layers, preserving their pillow structure, and locally in lenses embedded and deformed within the
710 mélange. (C) The pervasive deformation of the mélange is visible in its sedimentary layers, with a
711 dense network of macroscopic top-to-the-south mineralized shear zones deflecting the foliation and
712 offsetting sandstone lenses. (D) More localized zones of deformation are present along the
713 boundaries of the basalt lenses, including the pseudotachylyte-bearing one (PST). Note that the field
714 drawing in (D) is a mirror image of the actual outcrop, to keep the same N-S orientation as (B) and (C).

715 Figure 6: Kinematics of deformation in the Mugi mélange (stereoplots with blue background). On
716 each stereographic plot, the red plane corresponds to the average foliation, while planes with arrows
717 correspond to shear bands. The white stereoplot on the right shows the data of the pseudotachylyte-
718 bearing fault zone of Minami-Awa, which bounds the Mugi mélange unit (Kitamura, 2006; Kitamura
719 et al., 2005) The numbers on the map refer to outcrops. The average azimuth of slicken lines is
720 shown as the thick black ticks. Stereo diagrams are equal area, lower hemisphere.

721 Figure 7: Deformation structures within the Okitsu mélange (outcrop 220 – see Supp. Mat. for
722 location). The vertical foliation, composed of elongated sandstone lenses embedded in a shale matrix,
723 is crosscut by a dense network of shear bands with top-to-the-SSE sense of shear. Quartz
724 precipitation is in A) mostly distributed within fractures cutting across the sandstone lenses.
725 Alternately, in B), quartz precipitation is much more intense and quartz also precipitates along and in
726 the vicinity of the shear bands. A and B photographs, A' and B' corresponding sketches.

727 Figure 8: Network of shear bands deflecting the vertical sandstone lenses and the foliation of the
728 shale matrix within the Mugi mélange (outcrop 342 – see Supp. Mat. for location). Most of the shear
729 bands are filled with quartz.

730 Figure 9: Deformation microstructures in the Hyuga mélange (outcrop 147 – see Supp. Mat. for
731 location), from Raimbourg et al. (2014a). Lenses of sandstone, elongated parallel to the foliation
732 within the pelitic matrix, are boudinaged. Quartz precipitated as foliation-parallel lenses and in

733 tension cracks forming the necks of sandstone lenses. Both quartz and sandstone lenses are
734 deflected by top-to-the-SE shear bands.

735 Figure 10: Veining in mélanges in Okitsu (A), Mugi (B) and Hyuga (C) areas. Quartz veins form as
736 tension cracks perpendicular to stretching direction in rigid lenses of sandstones (blue arrows), and in
737 veins parallel to foliation S1 (red arrows). Samples references are respectively HN323, HN462 and
738 HN64 (see Supp. Mat. for location). Each sample is rotated to its actual dip.

739 Figure 11: Deformation within the mélange is made of a distributed network of shear zones, affecting
740 lenses of sedimentary material as well as precipitated quartz ("quartz veins"). Quartz precipitation
741 occurs (i) in fractures cutting across sandstone lenses, (ii) in the neck of boudinaged sandstone lenses
742 and (iii) in lenses elongated parallel to the main foliation (sample HN299 – see Supp. Mat. for
743 location).

744 Figure 12: Detail of a shear band cutting across elongated lenses of quartz and siltstone, within the
745 Hyuga mélange (sample HN299 – see Supp. Mat. for location). Quartz lenses are continuous across
746 the shear band and deflected by it. Most of the lenses in this pervasively deformed sample are not
747 composed of sedimentary, coarser-grained siltstone, but rather of lenses of precipitated quartz. The
748 two rectangles in the left picture correspond to Figure 13.

749 Figure 13: Optical microscope photographs, without (A, B) and with (A', B') crossed-nicols, of
750 deformation microstructures within the shear band in Figure 12. A-A') A network of microscale,
751 chlorite-filled shear zones ("Chl.") develop within the main shear zone. B-B') Quartz lenses elongated
752 within the shear band are pervasively affected by microcracking, apparent in the dense array of fluid
753 inclusion planes, shown as arrows, oriented perpendicular to the stretching direction. Quartz crystals
754 (B') are elongated preferentially parallel to the stretching direction.

755 Figure 14: Underplating models, with distributed (A) and localized (B) deformation. For the
756 "distributed underplating" model, in an initial stage (A_1), all the plate relative motion is

accommodated within the mélange. Because of strain or metamorphic hardening of the mélange, a localized slip zone forms within the basalt of the subducting plate (A_2) and connects to the upper boundary of the mélange to form a wedge-shape zone. In the resulting evolution (A_3 and A_4), this wedge of mélange stretches, to account, because of mass conservation, for the difference in flow resulting from thinner section in the wedge (velocity profiles in A_4'', corresponding to stage A_4). Mélange flowing through the wedge accommodates the geometrical thinning through the development of pervasive extensional shear zones, similar to the ones recorded in fossil mélange examples. Two successive stages of deformation are recorded in the mélange (model A), first layer-parallel shear (far from underplating zone), then extensional shear (during underplating).

Table 1: P-T conditions of deformation within the mélange units. Sample locations are given in decimal degrees. Temperatures were calculated from vitrinite reflectance according to the equations in Barker (1988), in agreement with the study of Laughland and Underwood (1993). Please note the slight difference in the reflectance values reported in the literature, either mean or maximum reflectance. RSCM temperatures were calculated from the calibration by Lahfid et al. (2010). Temperatures were calculated from illite crystallinity according to the equations in Hara and Kimura (2008).

Supplementary Material

Outcrop number	sample reference	Latitude (N)	Longitude (E)
220		33.203233	133.234406
342		33.683763	134.477061
147		32.409790	131.254973
111		32.431239	131.310953
112-113		32.430541	131.312791
116		32.416224	131.320819
202O		32.415133	131.278167
	HN64	32.594418	131.462973
	HN299	32.403317	131.279000
	HN323	33.203232	133.234406
	HN462	33.670679	134.449622

Supplementary Material: Outcrop and sample location, in decimal degrees.

References

Angelier, J., Barrier, E. and Chu, H.-T. (1986) Plate collision and paleostress trajectories in a fold-and-thrust belt: the Foothills of Taiwan. Tectonophysics 125, 161-178.

Angelier, J., Bergerat, F., Chu, H.-T. and Lee, T.-Q. (1990) Tectonic analysis and the evolution of a curved collision belt: The Hsiiehshan Range, northern Taiwan. Tectonophysics 183, 77-96.

Bachmann, R., Oncken, O., Glodny, J., Seifert, W., Georgieva, V. and Sudo, M. (2009) Exposed plate interface in the European Alps reveals fabric styles and gradients related to an ancient seismogenic coupling zone. J. Geophys. Res. 114, 1-23.

Bally, A.W., Gordy, P.L. and Stewart, G.A. (1966) Structure, seismic data and orogenic evolution of southern Canadian Rocky Mountains. Bull. Can. Pet. Geol. 14, 337-381.

Barker, C.E. (1988) Geothermics of petroleum systems: implication of the stabilization of kerogen thermal maturation after a geologically brief heating duration at peak temperature. U.S. Geological Survey Bulletin 1970, 26-29.

Barrier, E. and Angelier, J. (1986) Active collision in Eastern Taiwan: the Coastal Range. Tectonophysics 125, 39-72.

Bilek, S. and Lay, T. (2018) Subduction zone megathrust earthquakes. Geosphere 14, 1468-1500.

Byrne, T. and Fisher, D. (1990) Evidence for a weak and overpressured decollement beneath sediment-dominated accretionary prisms. J. Geoph. Res. 95, 9081-9097.

Chang, C.-P., Angelier, J. and Huang, C.-Y. (2000) Origin and evolution of a me´lange: the active plate boundary and suture zone of the Longitudinal Valley, Taiwan. Tectonophysics 325, 43-62.

Chapple, W.M. (1978) Mechanics of thin-skinned fold-and-thrusts belts. Geological society of America Bulletin 89, 1189-1198.

Charvet, J. (2013) Late Paleozoic–Mesozoic tectonic evolution of SW Japan: A review – Reappraisal of the accretionary orogeny and revalidation of the collisional model. J. Asian Earth Sci. 72, 88-101.

Charvet, J. and Fabbri, O. (1987) Vue générale sur l'orogenèse Shimanto et l'évolution tertiaire du Japon sud-ouest. Bull. Soc. Geol. France 8, 1171-1188 (in french with english abstract).

Chester, F.M. and Logan, J.M. (1986) Implications for mechanical properties of brittle faults from observations of the Punchbowl Fault Zone, California. Pure and Applied Geophysics 124, 79-106.

Chester, F.M., Rowe, C., Ujiie, K., Kirkpatrick, J., Regalla, C., Remitti, F., Moore, J.C., Toy, V., Wolfson-Schwehr, M., Bose, S., Kameda, J., Mori, J.J., Brodsky, E.E., Eguchi, N., Toczko, S. and Scientists, E.a.T. (2013) Structure and composition of the plate-boundary slip zone for the 2011 Tohoku-Oki earthquake. Science 342, 1208-1211.

Cloos, M. (1982) Flow melanges: Numerical modelling and geologic constraints on their origin in the Franciscan complex, California. Geological Society of America Bulletin 93, 330-345.

Cloos, M. and Shreve, R. (1988a) Subduction-channel model of prism accretion, melange formation, sediment subduction, and subduction erosion at convergent plate margins: 1. Background and description. Pure Appl. Geophys. 128, 455-500.

Cloos, M. and Shreve, R. (1988b) Subduction-channel model of prism accretion, melange formation, sediment subduction, and subduction erosion at convergent plate margins: 2. Implications and Discussion. Pure Appl. Geophys. 128, 501-545.

Connelly, W. (1978) Uyak Complex, Kodiak Islands, Alaska: A Cretaceous subduction complex. GSA Bull. 89, 755-769.

Cowan, D.S. (1974) Deformation and metamorphism of the Franciscan subduction zone complex northwest of Pacheco Pass, California. GSA Bull. 85, 1623-1634.

Cowan, D.S. (1985) Structural styles in Mesozoic and Cenozoic mélanges in the western Cordillera of North America. GSA Bull. 96, 451-462.
den Hartog, S.A.M., Niemeijer, A.R. and Spiers, C.J. (2012) New constraints on megathrust slip stability under subduction zone P–T conditions. Earth Planet. Sci. Lett. 353-354, 240-252.
den Hartog, S.A.M., Niemeijer, A.R. and Spiers, C.J. (2013) Friction on subduction megathrustfaults: Beyond the illite–muscovite transition. Earth Planet. Sci. Lett. 373, 8-19.
Den Hartog, S.A.M. and Spiers, C.J. (2013) Influence of subduction zone conditions and gouge composition on frictional slip stability of megathrust faults. Tectonophysics 600.
Den Hartog, S.A.M. and Spiers, C.J. (2014) A microphysical model for fault gouge friction applied to subduction megathrusts. J. Geophys. Res. 119, 1510-1529.
Dielforder, A., Vollstaedt, H., Vennemann, T.W., Berger, A. and Herwegh, M. (2015) Linking megathrust earthquakes to brittle deformation in a fossil accretionary complex. Nature Communications 6, 1-10.
Dieterich, J.H. (1994) A constitutive law for rate of earthquake production and its application to earthquake clustering. J. Geophys. Res. 99, 2601-2618.
Dragert, H., Wang, K. and James, T.S. (2001) A silent slip event on the deeper Cascadia subduction interface. Science 292, 1525-1528.
England, P.C. and Holland, T.J.B. (1979) Archimedes and the Tauern eclogites: the role of buoyancy in the preservation of exotic eclogite blocks. Earth Planet. Sci. Lett. 44, 287-294.
Evans, M.A. and Dunne, W.M. (1991) Strain factorization and partitioning in the North Mountain thrust sheet, central Appalachians, U.S.A. J. Struct. Geol. 13, 21-35.
Fagereng, A. and Den Hartog, S.A.M. (2017) Subduction megathrust creep governed by pressure solution and frictional–viscous flow. Nat. Geo. 10, 51-60.
Fagereng, A., Diener, J.F.A., Ellis, S. and Remitti, F. (2018) Fluid-related deformation processes at the up- and downdip limits of the subduction thrust seismogenic zone: What do the rocks tell us? GSA Spec. Pap. 534, 187-215.
Fagereng, A. and Harris, C. (2014) Interplay between fluid flow and fault–fracture mesh generation within underthrust sediments: Geochemical evidence from the Chrystalls Beach Complex, New Zealand. Tectonophysics 612-613, 147-157.
Fagereng, A., Remitti, F. and Sibson, R.H. (2011) Incrementally developed slickenfibers - geological record of repeating low stress-drop seismic events? Tectonophysics 510, 381-386.
Fagereng, A. and Sibson, R.H. (2010) Mélange rheology and seismic style. Geology 38, 751-754.
Faulkner, D.R., Jackson, C.A.L., Lunn, R.J., Schlische, R.W., Shipton, Z.K., Wibberley, C. and Withjack, M.O. (2010) A review of recent developments concerning the structure, mechanics and fluid flow properties of fault zones. J. Struct. Geol. 32, 1557-1575.
Faulkner, D.R., Lewis, A.C. and Rutter, E.H. (2003) On the internal structure and mechanics of large strike-slip fault zones: field observations of the Carboneras fault in southeastern Spain. Tectonophysics 367, 235-251.
Festa, A., Dilek, Y., Pini, G.A., Codegone, G. and Ogata, K. (2012) Mechanisms and processes of stratal disruption and mixing in the development of mélanges and broken formations: Redefining and classifying mélanges. Tectonophysics 568-569, 7-24.
Fisher, D. and Byrne, T. (1987) Structural evolution of underthrusted sediments, Kodiak Islands, Alaska. Tectonics 6, 775-793.
Fisher, D. and Byrne, T. (1990) The character and distribution of mineralized fractures in the Kodiak Formation, Alaska: Implications for fluid flow in an underthrust sequence. J. Geophys. Res. 95, 9069-9080.
Fisher, D.M. and Brantley, S.L. (1992) Models of quartz overgrowth and vein formation: deformation and episodic fluid flow in an ancient subduction zone. J. Geophys. Res. 97, 20,043-020,061.
Fisher, D.M. and Brantley, S.L. (2014) The role of silica redistribution in the evolution of slip instabilities along subduction interfaces: Constraints from the Kodiak accretionary complex, Alaska. J. Struct. Geol. 69B, 395-414.

872 Fisher, D.M., Brantley, S.L., Everett, M. and Dzonik, J. (1995) Cyclic fluid flow through a regionally
873 extensive fracture network within the Kodiak accretionary prism. J. Geophys. Res. 100, 12,881-
874 812,894.
875 Gratier, J.P., Guiguet, R., Renard, F., Jenatton, L. and Bernard, D. (2009) A pressure solution creep law
876 for quartz from indentation experiments. J. Geophys. Res. 114, 1-16.
877 Hara, H. and Kimura, K. (2008) Metamorphic cooling history of the Shimanto accretionary complex,
878 Kyushu, southwest Japan: Implications for the timing of out-of-sequence thrusting. Island Arc 17,
879 546-559.
880 Hara, H., Nakamura, Y., Hara, K., Kurihara, T., Mori, H., Iwano, H., Danhara, T., Sakata, S. and Hirata, T.
881 (2017) Detrital zircon multi-chronology, provenance, and low-grade metamorphism of the
882 Cretaceous Shimanto accretionary complex, eastern Shikoku, Southwest Japan: Tectonic evolution in
883 response to igneous activity within a subduction zone. Island Arc 26, 1-24.
884 Hashimoto, Y. and Kimura, G. (1999) Underplating process from melange formation to duplexing:
885 Example from the Cretaceous Shimanto Subbelt, Kii Peninsula, southwest Japan. Tectonics 18, 92-107.
886 Hashimoto, Y., Nakaya, T., Ito, M. and Kimura, G. (2006) Tectonolithification of sandstone prior to the
887 onset of seismogenic subduction zone: Evidence from tectonic mélange of the Shimanto Belt, Japan.
888 G-cubed 7, 1-7.
889 Homberg, C., Bergerat, F., Philippe, Y., Lacombe, O. and Angelier, J. (2002) Structural inheritance and
890 cenozoic stress fields in the Jura fold-and-thrust belt (France). Tectonophysics 357, 137-158.
891 Honda, G., Ishikawa, T., Hirono, T. and Mukoyoshi, H. (2011) Geochemical signals for determining the
892 slip‐weakening mechanism of an ancient megasplay fault in the Shimanto accretionary complex.
893 Geophys. Res. Lett. 38, 1-5.
894 Hyndman, R.D., Yamano, M. and Oleskevich, D.A. (1997) The seismogenic zone of subduction thrust
895 faults. The Island Arc 6, 244-260.
896 Ikari, M.J., Saffer, D.M. and Marone, C. (2007) Effect of hydration state on the frictional properties of
897 montmorillonite-based fault gouge. J. Geophys. Res. 112, 1-12.
898 Ikari, M.J., Saffer, D.M. and Marone, C. (2009) Frictional and hydrologic properties of clay-rich fault
899 gouge. J. Geophys. Res. 114, 1-18.
900 Ikesawa, E., Kimura, G., Sato, K., Ikehara-Ohmori, K., Kitamura, Y., Yamaguchi, A., Ujiie, K. and
901 Hashimoto, Y. (2005) Tectonic incorporation of the upper part of oceanic crust to overriding plate of
902 a convergent margin: An example from the Cretaceous-early Tertiary Mugi Melange, the Shimanto
903 Belt, Japan. Tectonophysics 401, 217-230.
904 Ikesawa, E., Sakaguchi, A. and Kimura, G. (2003) Pseudotachylyte from an ancient accretionary
905 complex: Evidence for melt generation during seismic slip along a master décollement? Geology 31,
906 637-640.
907 Imai, I., Teraoka, Y., Okumura, K. and Ono, K. (1975) Geological Map of Japan, 1:50,000, Mikado.
908 Geological Survey of Japan.
909 Kato, N. and Hirasawa, T. (1997) A numerical study on seismic coupling along subduction zones using
910 a laboratory-derived friction law. Phys. Earth Planet. Inter. 102, 51-68.
911 Kiminami, K., Kashiwagi, N. and Miyashita, S. (1992) Ocurrence and significance of in-situ greenstones
912 from the Mugi Formation in the Upper Cretaceous Shimanto Supergroup, eastern Shikoku, Japan.
913 Jour. Geol. Soc. Japan 98, 867-883.
914 Kimura, G., Hashimoto, C., Yamaguchi, A., Kitamura, Y. and Ujiie, K. (2016) Cretaceous-Neogene
915 accretionary units: Shimanto Belt, in: Moreno, T., Wallis, S., Kojima, T., Gibbons, W. (Eds.), The
916 Geology of Japan. The Geological Society of London, London, pp. 125-137.
917 Kimura, G. and Mukai, A. (1991) Underplated unit in an accretionary complex: melange of the
918 Shimanto Belt of eastern Shikoku, southwest Japan. Tectonics 10, 31-50.
919 Kitamura, Y. (2006) A fate of sediments in subduction zones, University of Tokyo. Univ. of Tokyo,
920 Tokyo, p. 159.
921 Kitamura, Y. and Kimura, G. (2012) Dynamic role of tectonic mélange during interseismic process of
922 plate boundary mega earthquakes. Tectonophysics 568-569, 39-52.

Kitamura, Y., Sato, K., Ikesawa, E., Ikehara-Ohmori, K., Kimura, G., Kondo, H., Ujiie, K., Onishi, C.T., Kawabata, K., Hashimoto, Y., Mukoyoshi, H. and Masago, H. (2005) Melange and its seismogenic roof decollement: A plate boundary fault rock in the subduction zone - An example from the Shimanto Belt, Japan. Tectonics 24, 1-15.
Kondo, H., Kimura, G., Masago, H., Ohmori-Ikehara, K., Kitamura, Y., Ikesawa, E., Sakaguchi, A., Yamaguchi, A. and Okamoto, S. (2005) Deformation and fluid flow of a major out-of-sequence thrust located at seismogenic depth in an accretionary complex: Nobeoka Thrust in the Shimanto Belt, Kyushu, Japan. Tectonics 24, 1-16.
Lahfid, A., Beyssac, O., Deville, E., Negro, F., Chopin, C. and Goffé, B. (2010) Evolution of the Raman spectrum of carbonaceous material in low-grade metasediments of the Glarus Alps (Switzerland). Terra Nova 22, 354-360.
Lapusta, N. and Rice, J.R. (2003) Nucleation and early seismic propagation of small and large events in a crustal earthquake model. J. Geophys. Res. 108, 1-18.
Laughland, M.M. and Underwood, M. (1993) Vitrinite reflectance and estimates of paleotemperature within the Upper Shimanto Group, Muroto Peninsula, Shikoku, Japan, in: Underwood, M. (Ed.), Thermal evolution of the Tertiary Shimanto Belt, southwest Japan: an example of ridge-trench interaction, pp. 25-43.
Liu, Y. and Rice, J.R. (2005) Aseismic slip transients emerge spontaneously in three-dimensional rate and state modeling of subduction earthquake sequences. J. Geophys. Res. 110, 1-14.
Liu, Y. and Rice, J.R. (2007) Spontaneous and triggered aseismic deformation transients in a subduction fault model. J. Geophys. Res. 112, 1-23.
Loveless, J.P. and Meade, B.J. (2010) Geodetic imaging of plate motions, slip rates, and partitioning of deformation in Japan. J. Geophys. Res. 115, 1-35.
Maltman, A., Labaume, P. and Housen, B. (1997) Structural geology of the decollement at the toe of the Barbados accretionary prism, in: Shipley, T.H., Ogawa, Y., Blum, P., Bahr, J.M. (Eds.), Proc. ODP, Sci. Results, 156, pp. 279-292.
Mancktelow, N.S. (1995) Nonlithostatic pressure during sediment subduction and the development and exhumation of high pressure metamorphic rocks. Journal of geophysical research 100, 571-583.
Matsumura, M., Hashimoto, Y., Kimura, G., Ohmori-Ikehara, K., Enjohji, M. and Ikesawa, E. (2003) Depth of oceanic-crust underplating in a subduction zone: Inferences from fluid-inclusion analyses of crack-seal veins. Geology 31, 1005-1008.
Meneghini, F., Di Toro, G., Rowe, C.D., Moore, J.C., Tsutsumi, A. and Yamaguchi, A. (2010) Record of mega-earthquakes in subduction thrusts: The black fault rocks of Pasagshak Point (Kodiak Island, Alaska). GSA Bull. 122, 1280-1297.
Meneghini, F., Marroni, M., Moore, J.C., Pandolfi, L. and Rowe, C.D. (2009) The processes of underthrusting and underplating in the geologic record: structural diversity between the Franciscan Complex (California), the Kodiak Complex (Alaska) and the Internal Ligurian Units (Italy). Geol. J. 44, 126-152.
Meneghini, F., Marroni, M. and Pandolfi, L. (2007) Fluid flow during accretion in sediment-dominated margins: Evidence of a high-permeability fossil fault zone from the Internal Ligurian accretionary units of the Northern Apennines, Italy. J. Struct. Geol. 29, 519-527.
Meneghini, F. and Moore, J.C. (2007) Deformation and hydrofracture in a subduction thrust at seismogenic depths: The Rodeo Cove thrust zone, Marin Headlands, California. GSA Bull. 119, 174-183.
Mittempergher, S., Cerchiari, A., Remitti, F. and Festa, A. (2018) From soft sediment deformation to fluid assisted faulting in the shallow part of a subduction megathrust analogue: the Sestola Vidiciatico tectonic Unit (Northern Apennines, Italy). Geol. Mag. 155, 438-450.
Moore, D.E. and Lockner, D.A. (2004) Crystallographic controls on the frictional behavior of dry and water-saturated sheet structure minerals. J. Geophys. Res. 109, 1-16.
Moore, J.C. and Wheeler, R.L. (1978) Structural fabric of a mélange, Kodiak Islands, Alaska. Am. J. Sci. 278, 739-765.

Moreno, M., Rosenau, M. and Oncken, O. (2010) 2010 Maule earthquake slip correlates with pre-seismic locking of Andean subduction zone. Nature 467, 198-204.
Mukoyoshi, H., Hirono, T., Hara, H., Sekine, K., Tsuchiya, N., Sakaguchi, A. and Soh, W. (2009) Style of fluid flow and deformation in and around an ancient out-of-sequence thrust: An example from the Nobeoka Tectonic Line in the Shimanto accretionary complex, southwest Japan. Island Arc 18, 333-351.
Mukoyoshi, H., Sakaguchi, A., Otsuki, K., Hirono, T. and Soh, W. (2006) Co-seismic frictional melting along an out-of-sequence thrust in the Shimanto accretionary complex. Implications on the tsunamigenic potential of splay faults in modern subduction zones. Earth Planet. Sci. Lett. 245, 330-343.
Murata, A. (1994) Duplex structures and red & green siliceous mudstones of the Paleogene Hyuga Group in the Shimanto Terrane, Kyushu, Southwest Japan. J. Struct. Geol. Jpn. 40, 21-29.
Murata, A. (1996) Nappe structures of the Shimanto terrane of the Mikado-Osuzuyama area in East Kyushu. Natural Science Research, Faculty of Integrated Arts and Sciences, The University of Tokushima 9, 49-61 (in japanese with english abstract).
Murata, A. (1997) Geological map of Miyazaki prefecture, 1:200,000. Miyazaki Prefectural Government.
Murata, A. (1998) Duplexes and low-angle nappe structures of the Shimanto terrane, southwest Japan. Memoir of Geological Society of Japan 50, 147-158 (in japanese with english abstract).
Murata, A. (1999) Low-angle nappe structures of the Shimanto terrane in Kyushu and Shikoku, southwest Japan. J. Struct. Geol. Jpn. 43, 61-67 (in japanese with english abstract).
Niemeijer, A.R. (2018) Velocity-dependent slip weakening by the combined operation of pressure solution and foliation development. Scientific Reports 8, 1-10.
Niemeijer, A.R. and Spiers, C.J. (2007) A microphysical model for strong velocity weakening in phyllosilicate-bearing fault gouges. J. Geophys. Res. 112.
Niemeijer, A.R., Spiers, C.J. and Peach, C.J. (2008) Frictional behaviour of simulated quartz fault gouges under hydrothermal conditions: Results from ultra-high strain rotary shear experiments. Tectonophysics 460, 288-303.
Obara, K., Hirose, H., Yamamizu, F. and Kasahara, K. (2004) Episodic slow slip events accompanied by non-volcanic tremors in southwest Japan subduction zone. Geophys. Res. Lett. 31, 1-4.
Obara, K. and Kato, A. (2016) Connecting slow earthquakes to huge earthquakes. Science 353, 253-257.
Okumura, K., Teraoka, Y., Imai, I., Hoshizumi, H., Ono, K. and Shishido, A. (2010) Geological Map of Japan, 1:50,000, Nobeoka. Geological Survey of Japan.
Oleskevich, D.A., Hyndman, R.D. and Wang, K. (1999) The updip and downdip limits to great subduction earthquakes: Thermal and structural models of Cascadia, south Alaska, SW Japan, and Chile. J. Geoph. Res. 104, 14965-14991.
Onishi, C.T. and Kimura, G. (1995) Change in fabric of mélange in the Shimanto Belt, Japan: Change in relative convergence? Tectonics 14, 1273-1289.
Onishi, C.T., Kimura, G., Hashimoto, Y., Ikehara-Ohmori, K. and Watanabe, T. (2001) Deformation history of tectonic melange and its relationship to the underplating process and relative plate motion: An example from the deeply buried Shimanto Belt, SW Japan. Tectonics 20, 376-393.
Ozawa, K., Suito, H. and Tobita, M. (2007) Occurrence of quasi-periodic slow-slip off the east coast of the Boso peninsula, Central Japan. Earth Planets Space 59, 1241-1245.
Palazzin, G., Raimbourg, H., Famin, V., Jolivet, L., Kusaba, Y. and Yamaguchi, A. (2016) Deformation processes at the down-dip limit of the seismogenic zone: The example of Shimanto accretionary complex. Tectonophysics 687, 28-43.
Palazzin, G., Raimbourg, H., Stünitz, H., Heilbronner, R., Neufeld, K. and Précigout, J. (2018) Evolution in H2O contents during deformation of polycrystalline quartz: an experimental study. J. Struct. Geol. 114, 95-110.
Peng, Z. and Gomberg, J. (2010) An integrated perspective of the continuum between earthquakes and slow-slip phenomena. Nature Geoscience 3, 599-607.

Raimbourg, H., Augier, R., Famin, V., Gadenne, L., Palazzin, G., Yamaguchi, A. and Kimura, G. (2014a) Long-term evolution of an accretionary prism: the case study of the Shimanto Belt, Kyushu, Japan. Tectonics 33, 1-24.
Raimbourg, H., Famin, V., Palazzin, G., Mayoux, M., Jolivet, L., Ramboz, C. and Yamaguchi, A. (2018) Fluid properties and dynamics along the seismogenic plate interface. Geosphere: Subduction top to bottom 2 14, 1-23.
Raimbourg, H., Famin, V., Palazzin, G., Sakaguchi, A., Yamaguchi, A. and Augier, R. (2017) Tertiary evolution of the Shimanto Belt (Japan): a large-scale collision in Early Miocene. Tectonics 36, 1-21.
Raimbourg, H., Jolivet, L. and Leroy, Y. (2007b) Consequences of progressive eclogitisation on crustal exhumation, a mechanical study. Geophys. J. Int. 168, 379-401.
Raimbourg, H., Thiery, R., Vacelet, M., Ramboz, C., Cluzel, N., Trong, E.L., Yamaguchi, A. and Kimura, G. (2014b) A new method of reconstituting the P-T conditions of fluid circulation in an accretionary prism (Shimanto, Japan) from microthermometry of methane-bearing aqueous inclusions. Geochim Cosmochim Ac 125, 96-109.
Raimbourg, H., Vacelet, M., Ramboz, C., Famin, V., Augier, R., Palazzin, G., Yamaguchi, A. and Kimura, G. (2015) Fluid circulation in the depths of accretionary prisms: an example of the Shimanto Belt, Kyushu, Japan. Tectonophysics 655, 161-176.
Ring, U., Ratschbacher, L., Frisch, W., Biehler, D. and Kralik, M. (1989) Kinematics of the Alpine plate-margin: structural styles, strain and motion along the Penninic- Austroalpine boundary in the Swiss-Austrian Alps. J. Geol. Soc. 146, 835-849.
Rowe, C.D., Meneghini, F. and Moore, J.C. (2011) Textural record of the seismic cycle: strain-rate variation in an ancient subduction thrust. Geol. Soc. Lond. Spec. Publ. 359, 77-95.
Rowe, C.D., Moore, J.C., Meneghini, F. and McKeirnan, A.W. (2005) Large-scale pseudotachylytes and fluidized cataclasites from an ancient subduction thrust fault. Geology 33, 937-940.
Rowe, C.D., Moore, J.C., Remitti, F. and IODP Expedition 343/343T Scientists (2013) The thickness of subduction plate boundary faults from the seafloor into the seismogenic zone. Geology 41, 991-994.
Ruina, A. (1983) Slip instability and state variable friction laws. J. Geophys. Res. 88, 10359-10370.
Saffer, D., Frye, K.M., Marone, C. and Mair, K. (2001) Laboratory results indicating complex and potentially unstable frictional behavior of smectite clay. Geophys. Res. Lett. 28, 2297-2300.
Saffer, D., Lockner, D.A. and McKiernan, A.W. (2012) Effects of smectite to illite transformation on the frictional strength and sliding stability of intact marine mudstones. Geophys. Res. Lett. 39, 1-6.
Saffer, D. and Marone, C. (2003) Comparison of smectite- and illite-rich gouge frictional properties: application to the updip limit of the seismogenic zone along subduction megathrusts. Earth Planet. Sci. lett. 215, 219-235.
Saffer, D. and Wallace, L.M. (2015) The frictional, hydrologic, metamorphic and thermal habitat of shallow slow earthquakes. Nature Geoscience 8, 594-600.
Saito, M., Kimura, K., Naito, K. and Sakai, A. (1996) Geological Map of Japan, 1:50,000, Shiibamura. Geological Survey of Japan.
Sakaguchi, A. (1999a) Thermal maturity in the Shimanto accretionary prism, southwest Japan, with the thermal change of the subducting slab: Fluid inclusion and vitrinite reflectance study. Earth Planet. Sci. Lett. 173, 61-74.
Sakaguchi, A. (1999b) Thermal structure and paleo-heat flow in the Shimanto accretionary prism, Southwest Japan. The Island Arc 8, 359-372.
Sakaguchi, A. (2003) Observation of the seismogenic fault in the Okitsu Melange, Shimanto Accretionary Complex and stick-slip of mineral cementation of shear experiment. J. Geography 112, 885-896.
Sakaguchi, A., Hashimoto, Y., Mukoyoshi, H., Yokota, T., Takagi, M. and Kikuchi, T. (2006) Seismogenic fault-rock and fluid flow in ancient subduction zone: Field guide of Okitsu, Kure and Yokonami Mélanges, Cretaceous Shimanto accretionary complex, Shikoku, Japan. J. Geol. Soc. Japan 112, 71-88 (in japanese).
Sakai, H. (1988) Origin of the Misaki Olistostrome Belt and re-examination fo the Takachiho Orogeny. J. Geol. Soc. Jpn. 94, 945-961.

Sakai, T. (1985) Geology of the Nichinan Group and the process of production of the outermargin olisthostrome belt of the Shimanto terrane, Mem. Symp. on formation of slump facies and their relationship to tectonics, some problems on the deformation of unconsolidated sediments. Tectonic Research Group of Japan, Tsukuba, pp. 95-116 (in Japanese with english abstract).
Sakai, T., Nishi, H., Saito, T., Nakaseko, K. and Nishimura, A. (1984) Microfossil stratigraphy of the Paleogene system in Kyushu Shimanto Belt, in: Saito, T., Okada, H., Kaiho, K. (Eds.), Biostratigraphy and international correlation of the Paleogene system in Japan. Yamagata University, pp. 95-112 (in Japanese with english abstract).
Sakamoto, T. (1977) Neogene systems, in: Tanaka, K., Nozawa, T. (Eds.), Geology and mineral resources of Japan. Geol. Survey of Japan, pp. 233-259.
Sample, J.C. and Fisher, D.M. (1986) Duplex accretion and underplating in an ancient accretionary complex, Kodiak Islands, Alaska. Geology 14, 160-163.
Sample, J.C. and Moore, J.C. (1987) Structural style and kinematics of an underplated slate belt, Kodiak and adjacent islands, Alaska. GSA Bull. 99, 7-20.
Sawai, M., Niemeijer, A.R., Hirose, T. and Spiers, C.J. (2017) Frictional properties of JFAST core samples and implications for slow earthquakes at the Tohoku subduction zone. Geophys. Res. Lett. 44, 8822-8831.
Schutjens, P.M.T.M. (1991) Experimental compaction of quartz sand at low effective stress and temperature conditions. J. Geol. Soc. 148, 527-539.
Schwartz, S. and Rokosky, J.M. (2007) Slow slip events and seismic tremor at circum-Pacific subduction zones. Rev. Geophys. 45, 1-32.
Segall, P. and Rice, J.R. (1995) Dilatancy, compaction, and slip instability of a fluid-infiltrated fault. J. Geophys. Res. 100, 22,155-122,171.
Shibata, T., Orihashi, Y., Kimura, G. and Hashimoto, Y. (2008) Underplating of mélange evidenced by the depositional ages: U–Pb dating of zircons from the Shimanto accretionary complex, southwest Japan. Island Arc 17, 376-393.
Shipboard Scientific Party (1991) Site 808, in: Taira, A., Hill, I., Firth, J.V., et al. (Eds.), Proc. ODP, Init. Repts, vol 131, pp. 71-269.
Shipboard Scientific Party (2001) Site 1174, in: Moore, G.F., Taira, A., Klaus, A., Becker, L., Boeckel, B., Cragg, B.A., Dean, A., Fergusson, C.L., Henry, P., Hirano, S., Hisamitsu, T., Hunze, S., Kastner, M., Maltman, A.J., Morgan, J.K., Murakami, Y., Saffer, D.M., Sanchez-Gomez, M., Screaton, E.J., Smith, D.C., Spivack, A.J., Steurer, J., Tobin, H.J., Ujiie, K., Underwood, M.B., Wilson, M. (Eds.), Proc. ODP, Init. Repts, College Station, TX (Ocean Drilling Program), pp. 1-149.
Shreve, R.L. and Cloos, M. (1986) Dynamics of sediment subduction, melange formation, and prism accretion. Journal of Geophysical Research 91, 10229-10245.
Sibson, R.H. (2003) Thickness of the seismic slip zone. Bull. Seism. Soc. Am. 93, 1169-1178.
Stuart, W.D. (1988) Forecast model for great earthquakes at the Nankai Trough subduction zone. Pure Appl. Geophys. 126, 619-641.
Sweeney, J.J. and Burnham, A.K. (1990) Evaluation of a simple model of vitrinite reflectance based on chemical kinetics. AAPG Bull. 74, 1559-1570.
Taira, A. (1981) The Shimanto Belt of southwest Japan and arc-trench sedimentary tectonics. Recent Progress of Natural Sciences in Japan 6, 147-162.
Taira, A., Katto, J., Tashiro, M., Okamura, M. and Kodama, K. (1988) The Shimanto Belt in Shikoku, Japan-Evolution of Cretaceous to Miocene accretionary prism. Modern Geology 12, 5-46.
Taira, A., Okamura, M., Katto, J., Tashiro, H., Saito, Y., Kodama, K., Hashimoto, M., Chiba, T. and Aoki, T. (1980a) Lithofacies and geologic age relationship within mélange zones of northern Shimanto Belt (Cretaceous), Kochi prefecture, in: Taira, A., Tashiro, H. (Eds.), Geology and paleontology of the Shimanto Belt. Rinyo Kosaikai Press, Kochi, pp. 319-389.
Taira, A., Tashiro, M., Okamura, M. and Katto, J. (1980b) The geology of the Shimanto Belt in Kochi prefecture, Shikoku, in: Taira, A., Tashiro, H. (Eds.), Geology and paleontology of the Shimanto Belt. Rinyo Kosaikai Press, Kochi, pp. 319-389.

Tanaka, K. (1977) Pre-Neogene tectonic division, in: Tanaka, K., Nozawa, T. (Eds.), Geology and mineral resources of Japan. Geol. Survey of Japan, pp. 20-44.
Tonai, S., Ito, S., Hashimoto, Y., Tamura, H. and Tomioka, N. (2016) Complete 40Ar resetting in an ultracataclasite by reactivation of a fossil seismogenic fault along the subducting plate interface in the Mugi Mélange of the Shimanto accretionary complex, southwest Japan. J. Struct. Geol. 89, 19-29.
Toriumi, M. and Teruya, J. (1988) Tectono-metamorphism of the Shimanto Belt. Modern Geology 12, 303-324.
Tse, S.T. and Rice, J.R. (1986) Crustal earthquake instability in relation to the depth variation of frictional slip properties. J. Geophys. Res. 91, 9452-9472.
Ujiie, K. (1997) Off-scraping accretionary process under the subduction of young oceanic crust: The Shimanto Belt of Okinawa, Ryukyu Arc. Tectonics 16, 305-322.
Ujiie, K., Hisamitsu, T. and Soh, W. (2000) Magnetic and structural fabrics of the melange in the Shimanto accretionary complex, Okinawa Island: Implication for strain history during decollement-related deformation. Journal of Geophysical Research 105, 25729-25741.
Ujiie, K., Saishu, H., Fagereng, A., Nishiyama, N., Otsubo, M., Masuyama, H. and Kagi, H. (2018) An explanation of episodic tremor and slow slip constrained by crack-seal veins and viscous shear in subduction mélange. Geophys. Res. Lett. 45, 5371-5379.
Ujiie, K., Yamaguchi, H., Sakaguchi, A. and Toh, S. (2007) Pseudotachylytes in an ancient accretionary complex and implications for melt lubrication during subduction zone earthquakes. J. Struct. Geol. 29, 599-613.
Vannucchi, P., Remitti, F. and Bettelli, G. (2008) Geological record of fluid flow and seismogenesis along an erosive subducting plate boundary. Nature 451, 699-703.
Vannucchi, P., Remitti, F., Bettelli, G., Boschi, C. and Dallai, L. (2010) Fluid history related to the early Eocene - middle Miocene convergent system of the Northern Apennines (Italy): Constraints from structural and isotopic studies. J. Geophys. Res. 115, 1-23.
Vannucchi, P., Sage, F., Morgan, J.P., Remitti, F. and Collot, J.-Y. (2012a) Toward a dynamic concept of the subduction channel at erosive convergent margins with implications for interplate material transfer. Geochemistry Geophysics Geosystems 13, 1-24.
Vannucchi, P., Sage, F., Morgan, J.P., Remitti, F. and Collot, J.-Y. (2012b) Toward a dynamic concept of the subduction channel at erosive convergent margins with implications for interplate material transfer. G-cubed 13, 1-24.
Vrojlik, P. (1987) Tectonically-driven fluid flow in the Kodiak accretionary complex, Alaska. Geology 15, 466-469.
Vrolijk, P., Myers, G. and Moore, J.C. (1988) Warm fluid migration along tectonic melanges in the Kodiak accretionary complex, Alaska. J. Geophys. Res. 93, 10313-10324.
Wakabayashi, J. (2011) Mélanges of the Franciscan Complex, California: Diverse structural settings, evidence for sedimentary mixing, and their connection to subduction processes. GSA Spec. Paper 480, 1-6.
Wibberley, C. and Shimamoto, T. (2003) Internal structure and permeability of major strike-slip fault zones: the Median Tectonic Line in Mie Prefecture, Southwest Japan. J. Struct. Geol. 25, 59-78.
Wu, J., Suppe, J., Lu, R. and Kanda, R. (2016) Philippine Sea and East Asian plate tectonics since 52Ma constrained by new subducted slab reconstruction methods. J. Geophys. Res. 121, 4670-4741.

Angelier, J., Barrier, E. and Chu, H.-T. (1986) Plate collision and paleostress trajectories in a fold-and-thrust belt: the Foothills of Taiwan. Tectonophysics 125, 161-178.
Angelier, J., Bergerat, F., Chu, H.-T. and Lee, T.-Q. (1990) Tectonic analysis and the evolution of a curved collision belt: The Hsiiehshan Range, northern Taiwan. Tectonophysics 183, 77-96.
Bachmann, R., Oncken, O., Glodny, J., Seifert, W., Georgieva, V. and Sudo, M. (2009) Exposed plate interface in the European Alps reveals fabric styles and gradients related to an ancient seismogenic coupling zone. J. Geophys. Res. 114, 1-23.
Bally, A.W., Gordy, P.L. and Stewart, G.A. (1966) Structure, seismic data and orogenic evolution of southern Canadian Rocky Mountains. Bull. Can. Pet. Geol. 14, 337-381.
Barker, C.E. (1988) Geothermics of petroleum systems: implication of the stabilization of kerogen thermal maturation after a geologically brief heating duration at peak temperature. U.S. Geological Survey Bulletin 1970, 26-29.
Barrier, E. and Angelier, J. (1986) Active collision in Eastern Taiwan: the Coastal Range. Tectonophysics 125, 39-72.
Bilek, S. and Lay, T. (2018) Subduction zone megathrust earthquakes. Geosphere 14, 1468-1500.
Byrne, T. and Fisher, D. (1990) Evidence for a weak and overpressured decollement beneath sediment-dominated accretionary prisms. J. Geoph. Res. 95, 9081-9097.
Chang, C.-P., Angelier, J. and Huang, C.-Y. (2000) Origin and evolution of a me´lange: the active plate boundary and suture zone of the Longitudinal Valley, Taiwan. Tectonophysics 325, 43-62.
Chapple, W.M. (1978) Mechanics of thin-skinned fold-and-thrusts belts. Geological society of America Bulletin 89, 1189-1198.
Charvet, J. (2013) Late Paleozoic–Mesozoic tectonic evolution of SW Japan: A review – Reappraisal of the accretionary orogeny and revalidation of the collisional model. J. Asian Earth Sci. 72, 88-101.
Charvet, J. and Fabbri, O. (1987) Vue générale sur l'orogenèse Shimanto et l'évolution tertiaire du Japon sud-ouest. Bull. Soc. Geol. France 8, 1171-1188 (in french with english abstract).
Chester, F.M. and Logan, J.M. (1986) Implications for mechanical properties of brittle faults from observations of the Punchbowl Fault Zone, California. Pure and Applied Geophysics 124, 79-106.
Chester, F.M., Rowe, C., Ujiie, K., Kirkpatrick, J., Regalla, C., Remitti, F., Moore, J.C., Toy, V., Wolfson-Schwehr, M., Bose, S., Kameda, J., Mori, J.J., Brodsky, E.E., Eguchi, N., Toczko, S. and Scientists, E.a.T. (2013) Structure and composition of the plate-boundary slip zone for the 2011 Tohoku-Oki earthquake. Science 342, 1208-1211.
Cloos, M. (1982) Flow melanges: Numerical modelling and geologic constraints on their origin in the Franciscan complex, California. Geological Society of America Bulletin 93, 330-345.
Cloos, M. and Shreve, R. (1988a) Subduction-channel model of prism accretion, melange formation, sediment subduction, and subduction erosion at convergent plate margins: 1. Background and description. Pure Appl. Geophys. 128, 455-500.
Cloos, M. and Shreve, R. (1988b) Subduction-channel model of prism accretion, melange formation, sediment subduction, and subduction erosion at convergent plate margins: 2. Implications and Discussion. Pure Appl. Geophys. 128, 501-545.
Connelly, W. (1978) Uyak Complex, Kodiak Islands, Alaska: A Cretaceous subduction complex. GSA Bull. 89, 755-769.
Cowan, D.S. (1974) Deformation and metamorphism of the Franciscan subduction zone complex northwest of Pacheco Pass, California. GSA Bull. 85, 1623-1634.
Cowan, D.S. (1985) Structural styles in Mesozoic and Cenozoic mélanges in the western Cordillera of North America. GSA Bull. 96, 451-462.
den Hartog, S.A.M., Niemeijer, A.R. and Spiers, C.J. (2012) New constraints on megathrust slip stability under subduction zone P–T conditions. Earth Planet. Sci. Lett. 353-354, 240-252.
den Hartog, S.A.M., Niemeijer, A.R. and Spiers, C.J. (2013) Friction on subduction megathrustfaults: Beyond the illite–muscovite transition. Earth Planet. Sci. Lett. 373, 8-19.
Den Hartog, S.A.M. and Spiers, C.J. (2013) Influence of subduction zone conditions and gouge composition on frictional slip stability of megathrust faults. Tectonophysics 600.

Den Hartog, S.A.M. and Spiers, C.J. (2014) A microphysical model for fault gouge friction applied to subduction megathrusts. J. Geophys. Res. 119, 1510-1529.
Dieterich, J.H. (1994) A constitutive law for rate of earthquake production and its application to earthquake clustering. J. Geophys. Res. 99, 2601-2618.
Dragert, H., Wang, K. and James, T.S. (2001) A silent slip event on the deeper Cascadia subduction interface. Science 292, 1525-1528.
England, P.C. and Holland, T.J.B. (1979) Archimedes and the Tauern eclogites: the role of buoyancy in the preservation of exotic eclogite blocks. Earth Planet. Sci. Lett. 44, 287-294.
Evans, M.A. and Dunne, W.M. (1991) Strain factorization and partitioning in the North Mountain thrust sheet, central Appalachians, U.S.A. J. Struct. Geol. 13, 21-35.
Fagereng, A. and Den Hartog, S.A.M. (2017) Subduction megathrust creep governed by pressure solution and frictional–viscous flow. Nat. Geo. 10, 51-60.
Fagereng, A., Diener, J.F.A., Ellis, S. and Remitti, F. (2018) Fluid-related deformation processes at the up- and downdip limits of the subduction thrust seismogenic zone: What do the rocks tell us? GSA Spec. Pap. 534, 187-215.
Fagereng, A. and Sibson, R.H. (2010) Mélange rheology and seismic style. Geology 38, 751-754.
Faulkner, D.R., Jackson, C.A.L., Lunn, R.J., Schlische, R.W., Shipton, Z.K., Wibberley, C. and Withjack, M.O. (2010) A review of recent developments concerning the structure, mechanics and fluid flow properties of fault zones. J. Struct. Geol. 32, 1557-1575.
Faulkner, D.R., Lewis, A.C. and Rutter, E.H. (2003) On the internal structure and mechanics of large strike-slip fault zones: field observations of the Carboneras fault in southeastern Spain. Tectonophysics 367, 235-251.
Festa, A., Dilek, Y., Pini, G.A., Codegone, G. and Ogata, K. (2012) Mechanisms and processes of stratal disruption and mixing in the development of mélanges and broken formations: Redefining and classifying mélanges. Tectonophysics 568-569, 7-24.
Fisher, D. and Byrne, T. (1987) Structural evolution of underthrusted sediments, Kodiak Islands, Alaska. Tectonics 6, 775-793.
Fisher, D. and Byrne, T. (1990) The character and distribution of mineralized fractures in the Kodiak Formation, Alaska: Implications for fluid flow in an underthrust sequence. J. Geophys. Res. 95, 9069-9080.
Fisher, D.M. and Brantley, S.L. (1992) Models of quartz overgrowth and vein formation: deformation and episodic fluid flow in an ancient subduction zone. J. Geophys. Res. 97, 20,043-020,061.
Fisher, D.M. and Brantley, S.L. (2014) The role of silica redistribution in the evolution of slip instabilities along subduction interfaces: Constraints from the Kodiak accretionary complex, Alaska. J. Struct. Geol. 69B, 395-414.
Gratier, J.P., Guiguet, R., Renard, F., Jenatton, L. and Bernard, D. (2009) A pressure solution creep law for quartz from indentation experiments. J. Geophys. Res. 114, 1-16.
Hara, H. and Kimura, K. (2008) Metamorphic cooling history of the Shimanto accretionary complex, Kyushu, southwest Japan: Implications for the timing of out-of-sequence thrusting. Island Arc 17, 546-559.
Hara, H., Nakamura, Y., Hara, K., Kurihara, T., Mori, H., Iwano, H., Danhara, T., Sakata, S. and Hirata, T. (2017) Detrital zircon multi-chronology, provenance, and low-grade metamorphism of the Cretaceous Shimanto accretionary complex, eastern Shikoku, Southwest Japan: Tectonic evolution in response to igneous activity within a subduction zone. Island Arc 26, 1-24.
Hashimoto, Y. and Kimura, G. (1999) Underplating process from melange formation to duplexing: Example from the Cretaceous Shimanto Subbelt, Kii Peninsula, southwest Japan. Tectonics 18, 92-107.
Hashimoto, Y., Nakaya, T., Ito, M. and Kimura, G. (2006) Tectonolithification of sandstone prior to the onset of seismogenic subduction zone: Evidence from tectonic mélange of the Shimanto Belt, Japan. G-cubed 7, 1-7.
Homberg, C., Bergerat, F., Philippe, Y., Lacombe, O. and Angelier, J. (2002) Structural inheritance and cenozoic stress fields in the Jura fold-and-thrust belt (France). Tectonophysics 357, 137-158.

Honda, G., Ishikawa, T., Hirono, T. and Mukoyoshi, H. (2011) Geochemical signals for determining the slip‐weakening mechanism of an ancient megasplay fault in the Shimanto accretionary complex. Geophys. Res. Lett. 38, 1-5.
Hyndman, R.D., Yamano, M. and Oleskevich, D.A. (1997) The seismogenic zone of subduction thrust faults. The Island Arc 6, 244-260.
Ikari, M.J., Saffer, D.M. and Marone, C. (2007) Effect of hydration state on the frictional properties of montmorillonite-based fault gouge. J. Geophys. Res. 112, 1-12.
Ikari, M.J., Saffer, D.M. and Marone, C. (2009) Frictional and hydrologic properties of clay-rich fault gouge. J. Geophys. Res. 114, 1-18.
Ikesawa, E., Kimura, G., Sato, K., Ikehara-Ohmori, K., Kitamura, Y., Yamaguchi, A., Ujiie, K. and Hashimoto, Y. (2005) Tectonic incorporation of the upper part of oceanic crust to overriding plate of a convergent margin: An example from the Cretaceous-early Tertiary Mugi Melange, the Shimanto Belt, Japan. Tectonophysics 401, 217-230.
Ikesawa, E., Sakaguchi, A. and Kimura, G. (2003) Pseudotachylyte from an ancient accretionary complex: Evidence for melt generation during seismic slip along a master décollement? Geology 31, 637-640.
Imai, I., Teraoka, Y., Okumura, K. and Ono, K. (1975) Geological Map of Japan, 1:50,000, Mikado. Geological Survey of Japan.
Kato, N. and Hirasawa, T. (1997) A numerical study on seismic coupling along subduction zones using a laboratory-derived friction law. Phys. Earth Planet. Inter. 102, 51-68.
Kimura, G., Hashimoto, C., Yamaguchi, A., Kitamura, Y. and Ujiie, K. (2016) Cretaceous-Neogene accretionary units: Shimanto Belt, in: Moreno, T., Wallis, S., Kojima, T., Gibbons, W. (Eds.), The Geology of Japan. The Geological Society of London, London, pp. 125-137.
Kimura, G. and Mukai, A. (1991) Underplated unit in an accretionary complex: melange of the Shimanto Belt of eastern Shikoku, southwest Japan. Tectonics 10, 31-50.
Kitamura, Y. (2006) A fate of sediments in subduction zones, University of Tokyo. Univ. of Tokyo, Tokyo, p. 159.
Kitamura, Y. and Kimura, G. (2012) Dynamic role of tectonic mélange during interseismic process of plate boundary mega earthquakes. Tectonophysics 568-569, 39-52.
Kitamura, Y., Sato, K., Ikesawa, E., Ikehara-Ohmori, K., Kimura, G., Kondo, H., Ujiie, K., Onishi, C.T., Kawabata, K., Hashimoto, Y., Mukoyoshi, H. and Masago, H. (2005) Melange and its seismogenic roof decollement: A plate boundary fault rock in the subduction zone - An example from the Shimanto Belt, Japan. Tectonics 24, 1-15.
Kondo, H., Kimura, G., Masago, H., Ohmori-Ikehara, K., Kitamura, Y., Ikesawa, E., Sakaguchi, A., Yamaguchi, A. and Okamoto, S. (2005) Deformation and fluid flow of a major out-of-sequence thrust located at seismogenic depth in an accretionary complex: Nobeoka Thrust in the Shimanto Belt, Kyushu, Japan. Tectonics 24, 1-16.
Lahfid, A., Beyssac, O., Deville, E., Negro, F., Chopin, C. and Goffé, B. (2010) Evolution of the Raman spectrum of carbonaceous material in low-grade metasediments of the Glarus Alps (Switzerland). Terra Nova 22, 354-360.
Lapusta, N. and Rice, J.R. (2003) Nucleation and early seismic propagation of small and large events in a crustal earthquake model. J. Geophys. Res. 108, 1-18.
Laughland, M.M. and Underwood, M. (1993) Vitrinite reflectance and estimates of paleotemperature within the Upper Shimanto Group, Muroto Peninsula, Shikoku, Japan, in: Underwood, M. (Ed.), Thermal evolution of the Tertiary Shimanto Belt, southwest Japan: an example of ridge-trench interaction, pp. 25-43.
Liu, Y. and Rice, J.R. (2005) Aseismic slip transients emerge spontaneously in three-dimensional rate and state modeling of subduction earthquake sequences. J. Geophys. Res. 110, 1-14.
Liu, Y. and Rice, J.R. (2007) Spontaneous and triggered aseismic deformation transients in a subduction fault model. J. Geophys. Res. 112, 1-23.

Loveless, J.P. and Meade, B.J. (2010) Geodetic imaging of plate motions, slip rates, and partitioning of deformation in Japan. J. Geophys. Res. 115, 1-35.
Maltman, A., Labaume, P. and Housen, B. (1997) Structural geology of the decollement at the toe of the Barbados accretionary prism, in: Shipley, T.H., Ogawa, Y., Blum, P., Bahr, J.M. (Eds.), Proc. ODP, Sci. Results, 156, pp. 279-292.
Mancktelow, N.S. (1995) Nonlithostatic pressure during sediment subduction and the development and exhumation of high pressure metamorphic rocks. Journal of geophysical research 100, 571-583.
Matsumura, M., Hashimoto, Y., Kimura, G., Ohmori-Ikehara, K., Enjohji, M. and Ikesawa, E. (2003) Depth of oceanic-crust underplating in a subduction zone: Inferences from fluid-inclusion analyses of crack-seal veins. Geology 31, 1005-1008.
Meneghini, F., Di Toro, G., Rowe, C.D., Moore, J.C., Tsutsumi, A. and Yamaguchi, A. (2010) Record of mega-earthquakes in subduction thrusts: The black fault rocks of Pasagshak Point (Kodiak Island, Alaska). GSA Bull. 122, 1280-1297.
Meneghini, F., Marroni, M., Moore, J.C., Pandolfi, L. and Rowe, C.D. (2009) The processes of underthrusting and underplating in the geologic record: structural diversity between the Franciscan Complex (California), the Kodiak Complex (Alaska) and the Internal Ligurian Units (Italy). Geol. J. 44, 126-152.
Meneghini, F. and Moore, J.C. (2007) Deformation and hydrofracture in a subduction thrust at seismogenic depths: The Rodeo Cove thrust zone, Marin Headlands, California. GSA Bull. 119, 174-183.
Moore, D.E. and Lockner, D.A. (2004) Crystallographic controls on the frictional behavior of dry and water-saturated sheet structure minerals. J. Geophys. Res. 109, 1-16.
Moore, J.C. and Wheeler, R.L. (1978) Structural fabric of a mélange, Kodiak Islands, Alaska. Am. J. Sci. 278, 739-765.
Moreno, M., Rosenau, M. and Oncken, O. (2010) 2010 Maule earthquake slip correlates with pre-seismic locking of Andean subduction zone. Nature 467, 198-204.
Mukoyoshi, H., Hirono, T., Hara, H., Sekine, K., Tsuchiya, N., Sakaguchi, A. and Soh, W. (2009) Style of fluid flow and deformation in and around an ancient out-of-sequence thrust: An example from the Nobeoka Tectonic Line in the Shimanto accretionary complex, southwest Japan. Island Arc 18, 333-351.
Mukoyoshi, H., Sakaguchi, A., Otsuki, K., Hirono, T. and Soh, W. (2006) Co-seismic frictional melting along an out-of-sequence thrust in the Shimanto accretionary complex. Implications on the tsunamigenic potential of splay faults in modern subduction zones. Earth Planet. Sci. Lett. 245, 330-343.
Murata, A. (1994) Duplex structures and red & green siliceous mudstones of the Paleogene Hyuga Group in the Shimanto Terrane, Kyushu, Southwest Japan. J. Struct. Geol. Jpn. 40, 21-29.
Murata, A. (1996) Nappe structures of the Shimanto terrane of the Mikado-Osuzuyama area in East Kyushu. Natural Science Research, Faculty of Integrated Arts and Sciences, The University of Tokushima 9, 49-61 (in japanese with english abstract).
Murata, A. (1997) Geological map of Miyazaki prefecture, 1:200,000. Miyazaki Prefectural Government.
Murata, A. (1998) Duplexes and low-angle nappe structures of the Shimanto terrane, southwest Japan. Memoir of Geological Society of Japan 50, 147-158 (in japanese with english abstract).
Murata, A. (1999) Low-angle nappe structures of the Shimanto terrane in Kyushu and Shikoku, southwest Japan. J. Struct. Geol. Jpn. 43, 61-67 (in japanese with english abstract).
Niemeijer, A.R. (2018) Velocity-dependent slip weakening by the combined operation of pressure solution and foliation development. Scientific Reports 8, 1-10.
Niemeijer, A.R. and Spiers, C.J. (2007) A microphysical model for strong velocity weakening in phyllosilicate-bearing fault gouges. J. Geophys. Res. 112.

1375 Niemeijer, A.R., Spiers, C.J. and Peach, C.J. (2008) Frictional behaviour of simulated quartz fault
1376 gouges under hydrothermal conditions: Results from ultra-high strain rotary shear experiments.
1377 Tectonophysics 460, 288-303.
1378 Obara, K., Hirose, H., Yamamizu, F. and Kasahara, K. (2004) Episodic slow slip events accompanied by
1379 non-volcanic tremors in southwest Japan subduction zone. Geophys. Res. Lett. 31, 1-4.
1380 Obara, K. and Kato, A. (2016) Connecting slow earthquakes to huge earthquakes. Science 353, 253-
1381 257.
1382 Okumura, K., Teraoka, Y., Imai, I., Hoshizumi, H., Ono, K. and Shishido, A. (2010) Geological Map of
1383 Japan, 1:50,000, Nobeoka. Geological Survey of Japan.
1384 Oleskevich, D.A., Hyndman, R.D. and Wang, K. (1999) The updip and downdip limits to great
1385 subduction earthquakes: Thermal and structural models of Cascadia, south Alaska, SW Japan, and
1386 Chile. J. Geoph. Res. 104, 14965-14991.
1387 Onishi, C.T. and Kimura, G. (1995) Change in fabric of mélange in the Shimanto Belt, Japan: Change in
1388 relative convergence? Tectonics 14, 1273-1289.
1389 Onishi, C.T., Kimura, G., Hashimoto, Y., Ikehara-Ohmori, K. and Watanabe, T. (2001) Deformation
1390 history of tectonic melange and its relationship to the underplating process and relative plate
1391 motion: An example from the deeply buried Shimanto Belt, SW Japan. Tectonics 20, 376-393.
1392 Ozawa, K., Suito, H. and Tobita, M. (2007) Occurrence of quasi-periodic slow-slip off the east coast of
1393 the Boso peninsula, Central Japan. Earth Planets Space 59, 1241-1245.
1394 Palazzin, G., Raimbourg, H., Famin, V., Jolivet, L., Kusaba, Y. and Yamaguchi, A. (2016) Deformation
1395 processes at the down-dip limit of the seismogenic zone: The example of Shimanto accretionary
1396 complex. Tectonophysics 687, 28-43.
1397 Palazzin, G., Raimbourg, H., Stünitz, H., Heilbronner, R., Neufeld, K. and Précigout, J. (2018) Evolution
1398 in H2O contents during deformation of polycrystalline quartz: an experimental study. J. Struct. Geol.
1399 114, 95-110.
1400 Peng, Z. and Gomberg, J. (2010) An integrated perspective of the continuum between earthquakes
1401 and slow-slip phenomena. Nature Geoscience 3, 599-607.
1402 Raimbourg, H., Augier, R., Famin, V., Gadenne, L., Palazzin, G., Yamaguchi, A. and Kimura, G. (2014a)
1403 Long-term evolution of an accretionary prism: the case study of the Shimanto Belt, Kyushu, Japan.
1404 Tectonics 33, 1-24.
1405 Raimbourg, H., Famin, V., Palazzin, G., Mayoux, M., Jolivet, L., Ramboz, C. and Yamaguchi, A. (2018)
1406 Fluid properties and dynamics along the seismogenic plate interface. Geosphere: Subduction top to
1407 bottom 2 14, 1-23.
1408 Raimbourg, H., Famin, V., Palazzin, G., Sakaguchi, A., Yamaguchi, A. and Augier, R. (2017) Tertiary
1409 evolution of the Shimanto Belt (Japan): a large-scale collision in Early Miocene. Tectonics 36, 1-21.
1410 Raimbourg, H., Jolivet, L. and Leroy, Y. (2007b) Consequences of progressive eclogitisation on crustal
1411 exhumation, a mechanical study. Geophys. J. Int. 168, 379-401.
1412 Raimbourg, H., Thiery, R., Vacelet, M., Ramboz, C., Cluzel, N., Trong, E.L., Yamaguchi, A. and Kimura,
1413 G. (2014b) A new method of reconstituting the P-T conditions of fluid circulation in an accretionary
1414 prism (Shimanto, Japan) from microthermometry of methane-bearing aqueous inclusions. Geochim
1415 Cosmochim Ac 125, 96-109.
1416 Raimbourg, H., Vacelet, M., Ramboz, C., Famin, V., Augier, R., Palazzin, G., Yamaguchi, A. and Kimura,
1417 G. (2015) Fluid circulation in the depths of accretionary prisms: an example of the Shimanto Belt,
1418 Kyushu, Japan. Tectonophysics 655, 161-176.
1419 Ring, U., Ratschbacher, L., Frisch, W., Biehler, D. and Kralik, M. (1989) Kinematics of the Alpine plate-
1420 margin: structural styles, strain and motion along the Penninic- Austroalpine boundary in the Swiss-
1421 Austrian Alps. J. Geol. Soc. 146, 835-849.
1422 Rowe, C.D., Meneghini, F. and Moore, J.C. (2011) Textural record of the seismic cycle: strain-rate
1423 variation in an ancient subduction thrust. Geol. Soc. Lond. Spec. Publ. 359, 77-95.
1424 Rowe, C.D., Moore, J.C., Meneghini, F. and McKeirnan, A.W. (2005) Large-scale pseudotachylytes and
1425 fluidized cataclasites from an ancient subduction thrust fault. Geology 33, 937-940.

Rowe, C.D., Moore, J.C., Remitti, F. and IODP Expedition 343/343T Scientists (2013) The thickness of subduction plate boundary faults from the seafloor into the seismogenic zone. Geology 41, 991-994.
Ruina, A. (1983) Slip instability and state variable friction laws. J. Geophys. Res. 88, 10359-10370.
Saffer, D., Frye, K.M., Marone, C. and Mair, K. (2001) Laboratory results indicating complex and potentially unstable frictional behavior of smectite clay. Geophys. Res. Lett. 28, 2297-2300.
Saffer, D., Lockner, D.A. and McKiernan, A.W. (2012) Effects of smectite to illite transformation on the frictional strength and sliding stability of intact marine mudstones. Geophys. Res. Lett. 39, 1-6.
Saffer, D. and Marone, C. (2003) Comparison of smectite- and illite-rich gouge frictional properties: application to the updip limit of the seismogenic zone along subduction megathrusts. Earth Planet. Sci. lett. 215, 219-235.
Saffer, D. and Wallace, L.M. (2015) The frictional, hydrologic, metamorphic and thermal habitat of shallow slow earthquakes. Nature Geoscience 8, 594-600.
Saito, M., Kimura, K., Naito, K. and Sakai, A. (1996) Geological Map of Japan, 1:50,000, Shiibamura. Geological Survey of Japan.
Sakaguchi, A. (1999a) Thermal maturity in the Shimanto accretionary prism, southwest Japan, with the thermal change of the subducting slab: Fluid inclusion and vitrinite reflectance study. Earth Planet. Sci. Lett. 173, 61-74.
Sakaguchi, A. (1999b) Thermal structure and paleo-heat flow in the Shimanto accretionary prism, Southwest Japan. The Island Arc 8, 359-372.
Sakaguchi, A. (2003) Observation of the seismogenic fault in the Okitsu Melange, Shimanto Accretionary Complex and stick-slip of mineral cementation of shear experiment. J. Geography 112, 885-896.
Sakaguchi, A., Hashimoto, Y., Mukoyoshi, H., Yokota, T., Takagi, M. and Kikuchi, T. (2006) Seismogenic fault-rock and fluid flow in ancient subduction zone: Field guide of Okitsu, Kure and Yokonami Mélanges, Cretaceous Shimanto accretionary complex, Shikoku, Japan. J. Geol. Soc. Japan 112, 71-88 (in japanese).
Sakai, H. (1988) Origin of the Misaki Olistostrome Belt and re-examination fo the Takachiho Orogeny. J. Geol. Soc. Jpn. 94, 945-961.
Sakai, T. (1985) Geology of the Nichinan Group and the process of production of the outermargin olisthostrome belt of the Shimanto terrane, Mem. Symp. on formation of slump facies and their relationship to tectonics, some problems on the deformation of unconsolidated sediments. Tectonic Research Group of Japan, Tsukuba, pp. 95-116 (in Japanese with english abstract).
Sakai, T., Nishi, H., Saito, T., Nakaseko, K. and Nishimura, A. (1984) Microfossil stratigraphy of the Paleogene system in Kyushu Shimanto Belt, in: Saito, T., Okada, H., Kaiho, K. (Eds.), Biostratigraphy and international correlation of the Paleogene system in Japan. Yamagata University, pp. 95-112 (in Japanese with english abstract).
Sakamoto, T. (1977) Neogene systems, in: Tanaka, K., Nozawa, T. (Eds.), Geology and mineral resources of Japan. Geol. Survey of Japan, pp. 233-259.
Sample, J.C. and Fisher, D.M. (1986) Duplex accretion and underplating in an ancient accretionary complex, Kodiak Islands, Alaska. Geology 14, 160-163.
Sample, J.C. and Moore, J.C. (1987) Structural style and kinematics of an underplated slate belt, Kodiak and adjacent islands, Alaska. GSA Bull. 99, 7-20.
Sawai, M., Niemeijer, A.R., Hirose, T. and Spiers, C.J. (2017) Frictional properties of JFAST core samples and implications for slow earthquakes at the Tohoku subduction zone. Geophys. Res. Lett. 44, 8822-8831.
Schutjens, P.M.T.M. (1991) Experimental compaction of quartz sand at low effective stress and temperature conditions. J. Geol. Soc. 148, 527-539.
Schwartz, S. and Rokosky, J.M. (2007) Slow slip events and seismic tremor at circum-Pacific subduction zones. Rev. Geophys. 45, 1-32.
Segall, P. and Rice, J.R. (1995) Dilatancy, compaction, and slip instability of a fluid-infiltrated fault. J. Geophys. Res. 100, 22,155-122,171.

Shibata, T., Orihashi, Y., Kimura, G. and Hashimoto, Y. (2008) Underplating of mélange evidenced by the depositional ages: U–Pb dating of zircons from the Shimanto accretionary complex, southwest Japan. Island Arc 17, 376-393.
Shipboard Scientific Party (1991) Site 808, in: Taira, A., Hill, I., Firth, J.V., et al. (Eds.), Proc. ODP, Init. Repts, vol 131, pp. 71-269.
Shipboard Scientific Party (2001) Site 1174, in: Moore, G.F., Taira, A., Klaus, A., Becker, L., Boeckel, B., Cragg, B.A., Dean, A., Fergusson, C.L., Henry, P., Hirano, S., Hisamitsu, T., Hunze, S., Kastner, M., Maltman, A.J., Morgan, J.K., Murakami, Y., Saffer, D.M., Sanchez-Gomez, M., Screaton, E.J., Smith, D.C., Spivack, A.J., Steurer, J., Tobin, H.J., Ujiie, K., Underwood, M.B., Wilson, M. (Eds.), Proc. ODP, Init. Repts, College Station, TX (Ocean Drilling Program), pp. 1-149.
Shreve, R.L. and Cloos, M. (1986) Dynamics of sediment subduction, melange formation, and prism accretion. Journal of Geophysical Research 91, 10229-10245.
Sibson, R.H. (2003) Thickness of the seismic slip zone. Bull. Seism. Soc. Am. 93, 1169-1178.
Stuart, W.D. (1988) Forecast model for great earthquakes at the Nankai Trough subduction zone. Pure Appl. Geophys. 126, 619-641.
Taira, A. (1981) The Shimanto Belt of southwest Japan and arc-trench sedimentary tectonics. Recent Progress of Natural Sciences in Japan 6, 147-162.
Taira, A., Katto, J., Tashiro, M., Okamura, M. and Kodama, K. (1988) The Shimanto Belt in Shikoku, Japan-Evolution of Cretaceous to Miocene accretionary prism. Modern Geology 12, 5-46.
Taira, A., Okamura, M., Katto, J., Tashiro, H., Saito, Y., Kodama, K., Hashimoto, M., Chiba, T. and Aoki, T. (1980a) Lithofacies and geologic age relationship within mélange zones of northern Shimanto Belt (Cretaceous), Kochi prefecture, in: Taira, A., Tashiro, H. (Eds.), Geology and paleontology of the Shimanto Belt. Rinyo Kosaikai Press, Kochi, pp. 319-389.
Taira, A., Tashiro, M., Okamura, M. and Katto, J. (1980b) The geology of the Shimanto Belt in Kochi prefecture, Shikoku, in: Taira, A., Tashiro, H. (Eds.), Geology and paleontology of the Shimanto Belt. Rinyo Kosaikai Press, Kochi, pp. 319-389.
Tanaka, K. (1977) Pre-Neogene tectonic division, in: Tanaka, K., Nozawa, T. (Eds.), Geology and mineral resources of Japan. Geol. Survey of Japan, pp. 20-44.
Tonai, S., Ito, S., Hashimoto, Y., Tamura, H. and Tomioka, N. (2016) Complete 40Ar resetting in an ultracataclasite by reactivation of a fossil seismogenic fault along the subducting plate interface in the Mugi Mélange of the Shimanto accretionary complex, southwest Japan. J. Struct. Geol. 89, 19-29.
Toriumi, M. and Teruya, J. (1988) Tectono-metamorphism of the Shimanto Belt. Modern Geology 12, 303-324.
Tse, S.T. and Rice, J.R. (1986) Crustal earthquake instability in relation to the depth variation of frictional slip properties. J. Geophys. Res. 91, 9452-9472.
Ujiie, K. (1997) Off-scraping accretionary process under the subduction of young oceanic crust: The Shimanto Belt of Okinawa, Ryukyu Arc. Tectonics 16, 305-322.
Ujiie, K., Hisamitsu, T. and Soh, W. (2000) Magnetic and structural fabrics of the melange in the Shimanto accretionary complex, Okinawa Island: Implication for strain history during decollement-related deformation. Journal of Geophysical Research 105, 25729-25741.
Ujiie, K., Saishu, H., Fagereng, A., Nishiyama, N., Otsubo, M., Masuyama, H. and Kagi, H. (2018) An explanation of episodic tremor and slow slip constrained by crack-seal veins and viscous shear in subduction mélange. Geophys. Res. Lett. 45, 5371-5379.
Ujiie, K., Yamaguchi, H., Sakaguchi, A. and Toh, S. (2007) Pseudotachylytes in an ancient accretionary complex and implications for melt lubrication during subduction zone earthquakes. J. Struct. Geol. 29, 599-613.
Vannucchi, P., Remitti, F. and Bettelli, G. (2008) Geological record of fluid flow and seismogenesis along an erosive subducting plate boundary. Nature 451, 699-703.
Vannucchi, P., Remitti, F., Bettelli, G., Boschi, C. and Dallai, L. (2010) Fluid history related to the early Eocene - middle Miocene convergent system of the Northern Apennines (Italy): Constraints from structural and isotopic studies. J. Geophys. Res. 115, 1-23.

Vannucchi, P., Sage, F., Morgan, J.P., Remitti, F. and Collot, J.-Y. (2012a) Toward a dynamic concept of the subduction channel at erosive convergent margins with implications for interplate material transfer. Geochemistry Geophysics Geosystems 13, 1-24.
Vannucchi, P., Sage, F., Morgan, J.P., Remitti, F. and Collot, J.-Y. (2012b) Toward a dynamic concept of the subduction channel at erosive convergent margins with implications for interplate material transfer. G-cubed 13, 1-24.
Vrojlik, P. (1987) Tectonically-driven fluid flow in the Kodiak accretionary complex, Alaska. Geology 15, 466-469.
Wakabayashi, J. (2011) Mélanges of the Franciscan Complex, California: Diverse structural settings, evidence for sedimentary mixing, and their connection to subduction processes. GSA Spec. Paper 480, 1-6.
Wibberley, C. and Shimamoto, T. (2003) Internal structure and permeability of major strike-slip fault zones: the Median Tectonic Line in Mie Prefecture, Southwest Japan. J. Struct. Geol. 25, 59-78.
Wu, J., Suppe, J., Lu, R. and Kanda, R. (2016) Philippine Sea and East Asian plate tectonics since 52Ma constrained by new subducted slab reconstruction methods. J. Geophys. Res. 121, 4670-4741.

A Tobacco leaf GIPC

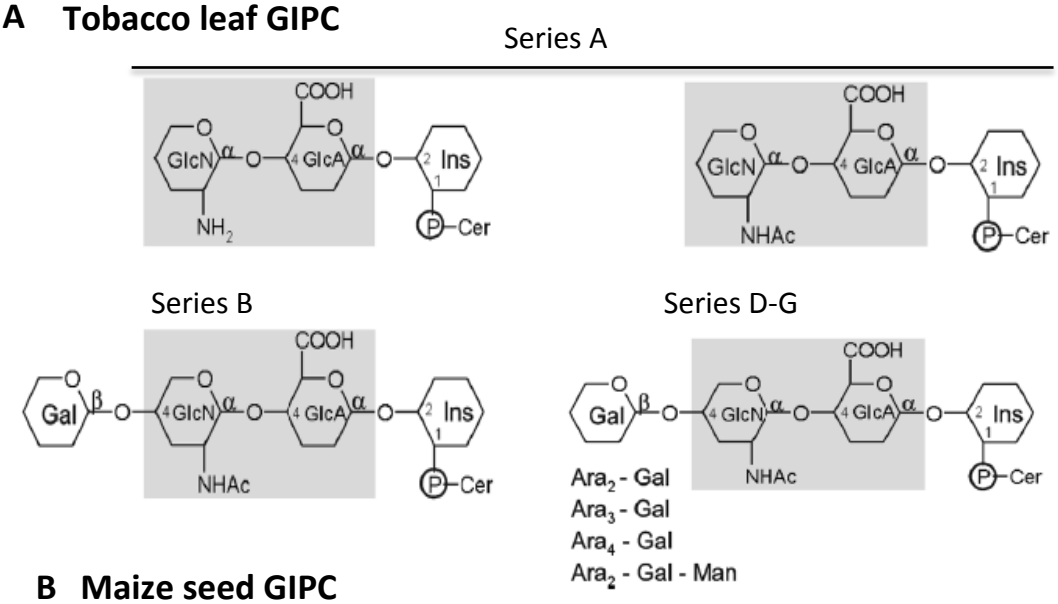

B Maize seed GIPC

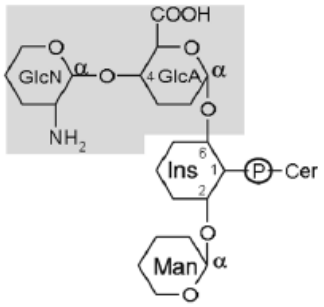

Figure 1: Determined structures of GIPC glycosidic polar head from tobacco and maize.

A, tobacco GIPC of series A are major in tobaco leaves (top) with glucuronic acid (GlcA) and either glucosamine (GlcN) or N-acetyl glucosamine (GlcNAc). Other minor polar head of series B and higher glycosylated GIPC with arabinoase (Ara), galactose (Gal) and Manose (Man) have been identified, but the precise structure remains to be determined. Grey part is the conserved glycan moitie of glucuronic-Hex. Cer indicates the ceramide moitie, in tobacco, with t18:0 and t18:1 for LCB, and VLCFA mostly alpha 2-hydroxylated ; B, GIPC found in corn seeds with branched polar head

A, Free phytosterols

Cholesterol

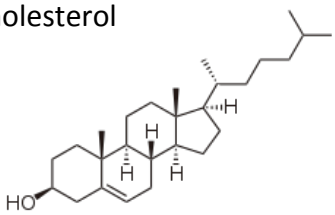

ß-Sitosterol

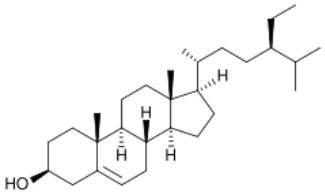

Stigmasterol

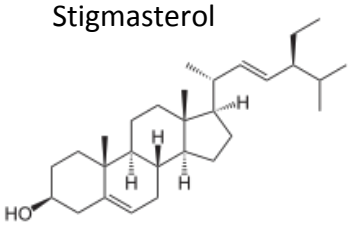

α-Spinasterol

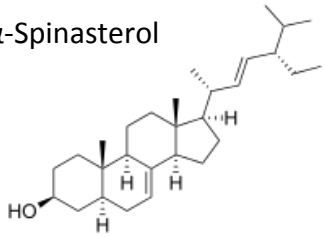

Campesterol

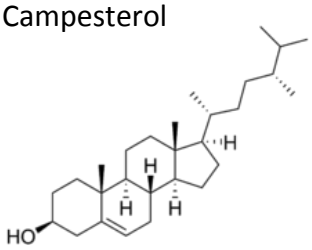

Fucosterol

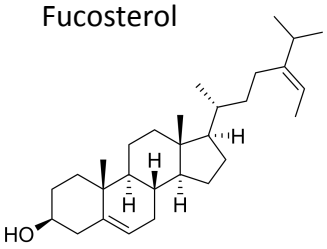

B, Phytostanol

ß-Sitostanol

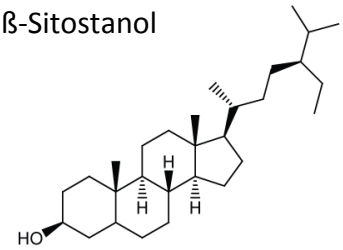

C, Conjugated phytosterols

ß-D-Glucosyl sitosterol

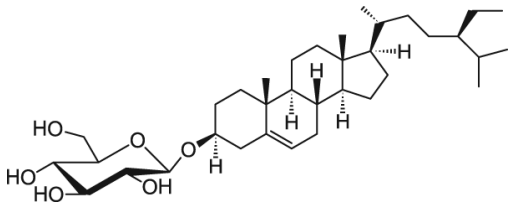

Palmitate ß-D-Glucosyl sitosterol

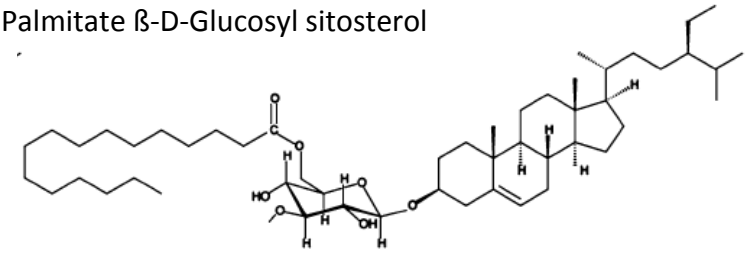

Figure 2: Structures of specific plasma membrane phytosterols compared with animal cholesterol.

A, free phytosterols ; B, phytostanol ; C, conjugated phytosterols.

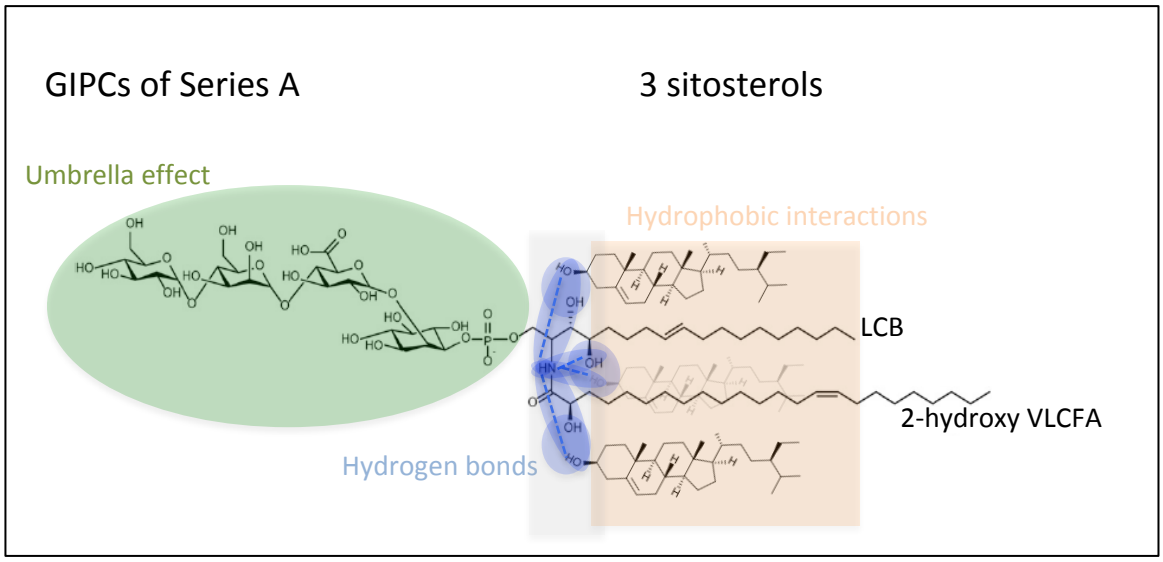

Figure 3: Biophysical features involved between a GIPC of series A and three molecules of sitosterols. These interactions are important for nanodomain formations in the PM. LCB, Long Chain Base; VLCFA, Very Long Chain Fatty Acid.

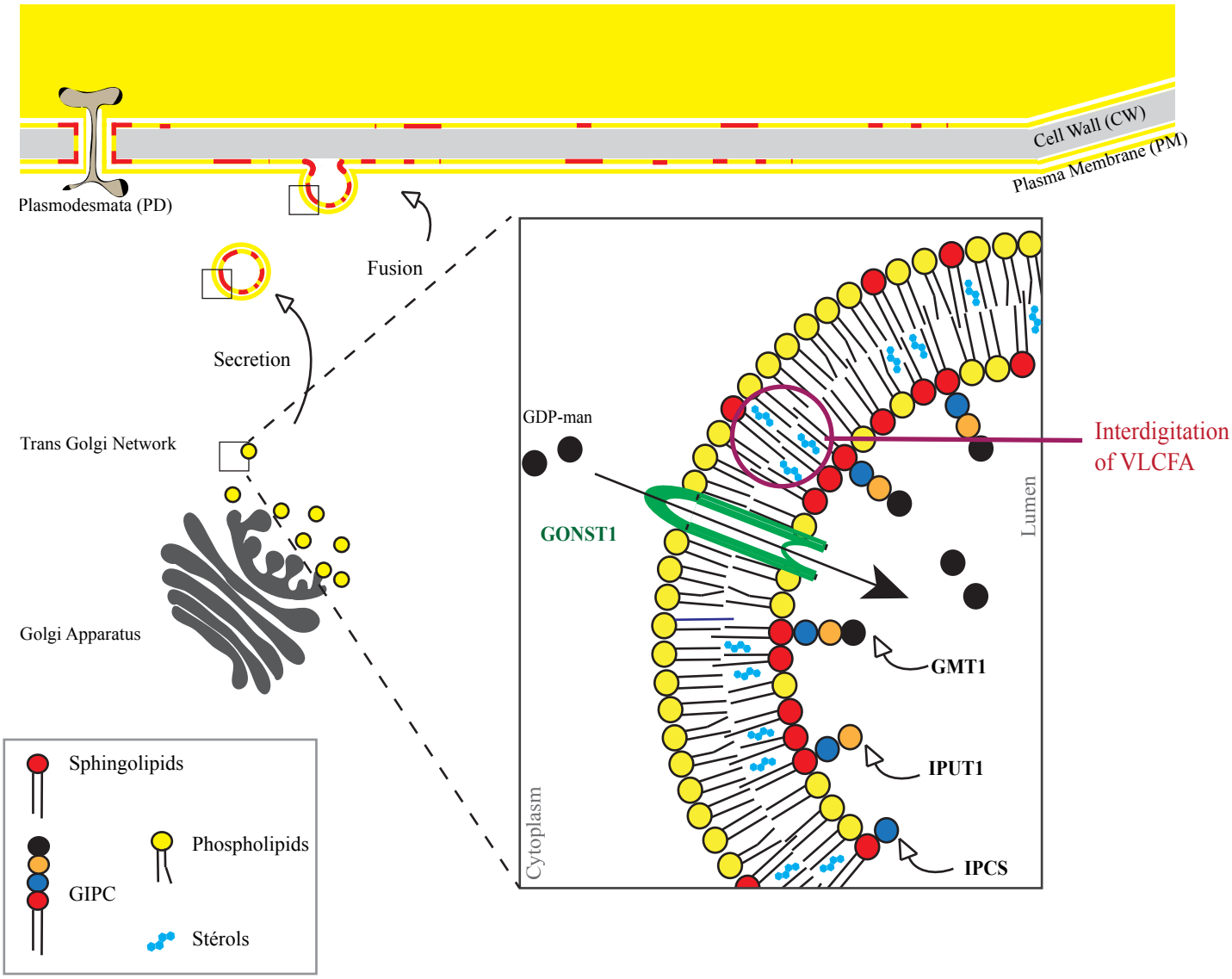

Figure 4: Formation of GIPC- and sterol-enriched domains along the secretory pathway.
GIPCs are synthesized in the lumen of the trans Golgi network (TGN) by grafting on the ceramide sequentially inositol-phosphate (IPCS, inositolphosphorylceramide synthase), glucuronic acid (IPUT1, inositol phosphorylceramide glucuronosyltransferase) and mannose (GMT1, GIPC mannosyl-transferase1). Golgi-localized nucleotide sugar transporter (GONST1) is responsible for the import of GDP-mannose to fuel GIPC synthesis. After vesicular fusion to the PM, GIPC polar heads face the apoplasm. Polyglycosylated GIPCs form nanodomains in the PM (in red).

Table 1: Examples of inhibitors used to modify *in vivo* the pools of lipids, and some recent related references.

The used concentration of the inhibitors is indicative, and must be tested for each plant species or tissues. To address the modification of the PM lipid pool, a phase partition to purify PM vesicles must be conducted coupled with a dedicated lipidomic approach. PLD, Phospholipase D; PLC, Phospholipase C, DAG, Diacylglycerol; VLCFAs, Very Long Chain Fatty Acids; HMG-CoA reductase, 3-hydroxy-3-methyl-glutaryl-coenzyme A reductase.

	Inhibitors of:	**Name**	**References**
Phosphoinositides	PI3-Kinase (50-100 µM)	LY-294002	[398]
	PI3P 5-Kinase (1 µM)	YM-201636	[399]
	PI4-Kinase (30-60 µM)	Phenylarsine oxide (PAO)	[117] [398]
	PI3-Kinase (1 µM)	Wortmannin	[283] [31]
	PI3-Kinase + PI4-Kinase (30 µM)	Wortmannin	
Sphingolipids	Ceramide synthase (1 µM)	Fumonisin B1 (1 mg)	[400] [401]
	Glucosylceramide synthase (50 µM)	DL-THREO-PDMP	[402]
	VLCFAs / sphingolipid (50-100 nM)	Metazachlor	[235]
	Serine palmitoyltransferase (SPT)	Myriocin	[56] [403]
	Inositol phosphorylceramide synthase (fungi)	Aureobasidin A	[404]
Diacylglycerol/ Phosphatidic Acid	Lyso PA Acyl transferase	CI-976	[405-407]
	PLD-derived PA formation (50 µM)	(R)-(+)-Propanolol hydrochloride	[408]
	PLD-derived PA formation (0.2-0.4%)	1- butanol	[409] [410]
	PLC-derived DAG formation (5 µM)	U73122 (active analog)	[31] [411]
	PLC-derived DAG formation (5 µM)	U73343 (inactive analog)	[411]
	PLC-derived DAG formation (50 µM)	Edelfosine	[283]
	DAG-Kinase (50 µM)	R59022	[283]
Sterols	Cyclopropylsterol isomerase 1, CPI1	Fenpropimorph	[7] [175] [162]
	HMG-CoA reductase	Lovastatin	[7]